REPORT DOCUMENTATION PAGE

AFRL-SR-AR-TR-06-0178

1. AGENCY USE ONLY *(Leave blank)*	2. REPORT DATE	3. REP
		01 Aug 2005 - 31 May 2006 FINAL

4. TITLE AND SUBTITLE
LASER INITIATION AND RADIOFREQUENCY SUSTAINMENT OF SEEDED AIR PLASMAS

5. FUNDING NUMBERS
2301/EX
61102F

6. AUTHOR(S)
DR SCHARER

7. PERFORMING ORGANIZATION NAME(S) AND ADDRESS(ES)
UNIVERSITY OF WISCONSIN
RESEARCH AND SPONSORED PROGRAMS
750 UNIVERSITY AVE
MADISON WI 53706-1411

8. PERFORMING ORGANIZATION REPORT NUMBER

9. SPONSORING/MONITORING AGENCY NAME(S) AND ADDRESS(ES)
AFOSR/NE
4015 WILSON BLVD
SUITE 713
ARLINGTON VA 22203
Dr Robert Barker

10. SPONSORING/MONITORING AGENCY REPORT NUMBER
F49620-03-1-0252

11. SUPPLEMENTARY NOTES

12a. DISTRIBUTION AVAILABILITY STATEMENT
DISTRIBUTION STATEMENT A: Unlimited

12b. DISTRIBUTION CODE

13. ABSTRACT *(Maximum 200 words)*

We have carried out research on hihg density (10 11 -4x10 13), large volume (500 -2500 cc), high-pressure (20-760 Torr), laser initiated plasma produced in nitrogen, argon and air. The low ionization energy organic gas (TMAE) laser-initiated seed plasmas create an initial condition that is used for plasma sustainment at much lower radiofrequency (RF) power levels (0.4 - 3 W/cc) than is the case for RF initiation alone.

14. SUBJECT TERMS			15. NUMBER OF PAGES
			16. PRICE CODE
17. SECURITY CLASSIFICATION OF REPORT	18. SECURITY CLASSIFICATION OF THIS PAGE	19. SECURITY CLASSIFICATION OF ABSTRACT	20. LIMITATION OF ABSTRACT
Unclassified	Unclassified	Unclassified	UL

Final Progress Report

Laser Initiation and Radiofrequency Sustainment of Seeded Air Plasmas

AFOSR Grant No. F49620-03-1-0252
May 1, 2003 - April 30, 2006

Professor J. E. Scharer, Principal Investigator
Department of Electrical and Computer Engineering
University of Wisconsin, Madison, WI 53706
Email: scharer@engr.wisc.edu

Laser Initiation and Radiofrequency Sustainment of Seeded Air Plasmas

Professor J. E. Scharer, Principal Investigator
Department of Electrical and Computer Engineering, University of Wisconsin, Madison, WI 53706

Abstract

We have carried out research on high density (10^{11}~$4x10^{13}$), large volume (500-2500 cc), high-pressure (20-760 Torr), laser initiated plasmas produced in nitrogen, argon and air. The low ionization energy organic gas (TMAE) laser-initiated seed plasmas create an initial condition that is used for plasma sustainment at much lower radiofrequency (RF) power levels (0.4 - 3 W/cc) than is the case for RF initiation alone. These plasmas have potential applications in the areas of materials processing, radar cross section reduction, supersonic drag reduction and biological decontamination. The 20 ns laser pulse provides a plasma lifetime in the several μs range that remains above 3×10^{12}/cc for 0.3 μs in air that provides a good plasma load for pulsed power RF sustainment. We have developed new techniques for measurement of plasma impedance and greatly improved matching between our laser initiated and RF sustained plasma conditions. Our results show that the UV laser formed plasmas allow RF sustainment at high pressures at much lower power levels and the RF penetrates further into the laser plasma to create a larger volume, higher density, lower required RF power density level sustainment than with RF alone. We have also demonstrated that the plasma resistive and inductive reactance can be accurately measured on a single pulse. The matching capacitors are then adjusted so that RF reflections are reduced to levels as low as 3 %. We have carried out temporal measurements of the broad emission spectra from the initial TMAE plasma to the high pressure gas plasma occurring later in the RF pulse. We have also carried out experiments on magnetized RF plasma sources to examine enhanced RF wave penetration for different gases, utilizing Langmuir probe, laser, optical spectroscopy, plasma wave, and interferometer diagnostics to measure the plasma electron velocity distribution function and density profiles. We have applied for and successfully obtained an AFOSR DURIP grant that will further enhance our experimental laser, spectroscopic and RF diagnostic capabilities that will allow us to expand our research and contribute to the MURI on the Nanotechnology of Microwave Breakdown. We have contributed material on High Frequency Air Plasma Production and a section on mm wave techniques to the Diagnostic Chapter for the book entitled *Non-Equilibrium Air Plasmas* that was published by the IOP. Three Ph. D. program graduate students participating in the research, two published and one submitted journal publications and ten conference presentations are also described.

Table of Contents

I. Introduction

High-pressure, inductively-coupled plasmas (ICP) have been used for a variety of scientific and industrial applications over a large gas pressure range from 50 Torr up to and beyond atmospheric pressures. For this plasma source, a helical antenna coil is used to couple radiofrequency (rf) power to the plasma using a capacitive impedance matching network. The applications of these plasmas require high-density (~ $10^{11\text{-}13}$ cm^{-3}), uniform plasmas over large volumes (~1000-5000 cm^3) with a reduced rf power budget. Atmospheric pressure plasmas can be used in open space for a variety of applications including materials processing [1], biological decontamination [2], microwave reflector and absorber [3], [4], and modification of the radar cross section and signature of an aircraft [5]. An up-to-date summary of atmospheric plasmas is available in a recent book entitled *Non-Equilibrium Air Plasmas at Atmospheric Pressure* [6]. One of the major issues associated with such high-pressure discharges is the high power budget required to initiate and sustain large volumes of these discharges at high density. The minimum theoretical power density per unit volume required to initiate and sustain an air plasma density of 10^{13} cm^{-3} at sea level (760 Torr) has been calculated to be 9 kW/cm^3 [7].

At higher gas pressures (10 Torr and above), the discharge kinetics are complicated, due in part to the increased role of two- and three-body collision processes. In addition to the role of atomic and molecular ions at low pressures, new charged and neutral species play an important role at high pressures. At higher gas pressures the electron-neutral collision rate increases, such that the primary collisions are between electrons and neutral molecules and the electron temperature is closer to the local neutral gas temperature [6]. As a result there is a decrease in the mean electron temperature at constant radiofrequency (rf) power and fewer high-energy electrons. Since the ionization efficiency is sensitive to the electron temperature, the reduction of higher energy electrons at higher gas pressures results in a lower production rate of electron-ion pairs.

The collisional ($\nu >> \omega_{rf}$). skin depth for rf penetration in an unmagnetized plasma [8] is $\delta = \sqrt{2}\ (c/\omega_p)(\nu/\omega_{rf})^{1/2}$ (where ν is the electron collision rate, c is the speed of light in vacuum, ω_{rf} is the rf frequency (13.56 MHz for our case), and ω_p is the electron plasma frequency.

The skin depth is larger for higher collision frequencies, lower densities, and lower rf frequencies. The rf penetration, field strength, and ionization at a given plasma density and collision rate will be larger for lower rf frequencies than for microwaves [9], [10].

In a classic experiment, Eckert *et al.* [11] created an atmospheric pressure plasma by initiating the discharge at a lower pressure (1 Torr) in both argon and air and slowly raising the pressure over time. They studied the emission spectrum produced by the high-pressure plasma and determined the plasma density and temperature. Following the work of Babat [12], they created a plasma using an inductive coil at a lower pressure and slowly increased the neutral pressure and rf power until they could open the plasma chamber to the atmosphere. To protect the quartz chamber from heat damage and to help stabilize the discharge, the gas was injected in a vortex, essentially forming a thermal gas barrier between the hot plasma and the chamber wall. The coupled power required to maintain the discharge was 18-50 kW at 4 MHz, sufficient to create the plasma at lower pressure and sustain it up to atmospheric pressure with a volume of about 2500 cubic centimeters (7-20 Watts / cm^3). The time scale for creating the high-pressure plasma from the initial low-pressure discharge was several minutes. There is current substantial interest in the fast initiation (milliseconds) of large-volume (greater than 1000 cm^3), high-density (10^{12}-10^{13} cm^{-3}) discharges at atmospheric pressures (50-760 Torr), corresponding to altitudes of 60,000 ft down to sea level, with minimal steady-state rf power. The power required in an experiment to ionize and initiate an inductively coupled rf plasma in atmospheric pressure air at a density of 10^{13} cm^{-3} will be much higher than the theoretical minimum power level (~ 9 kW/ cm^3). For an atmospheric pressure plasma arc torch, a 300 kV potential was required to initiate a discharge, whereas only 100 V is needed to maintain the discharge with operating currents of 200-600 Amps [13], [14]. Therefore, there is a need for an alternative scheme to reduce the power budget required to initiate and sustain the discharge at high gas pressures. We envisioned that if we could ionize a seed gas with a low ionization energy such as tetrakis (dimethylamino) ethylene (TMAE) (6.1 eV ionization potential) by ultraviolet laser or flashtube photon absorption [15], [16], [17] then we could efficiently couple electrodeless radiofrequency power to the plasma at high gas pressures and sustain the plasma at greatly reduced rf power levels.

We have focused on developing an electrodeless method for creating a large-volume (greater than 500 cm^3) seed plasma using UV photoionization to provide a good load for efficient rf coupling at low power levels via pulsed inductively-coupled sources. Previous experiments [15], [16], [17] have shown that a high initial density TMAE plasma ($10^{12\text{-}13}$ cm^{-3}) of long axial extent (~ 100 cm) can be efficiently created by a 193 nm laser in 760 Torr of nitrogen, air, oxygen, or argon. We thought that we might be able to create a steady-state high pressure plasma that projects well away from the antenna by this means that could not be obtained by RF alone. The initial plasma ionization also provides a plasma load to the inductive antenna, resulting in a good impedance match to the rf generator with reduced reflections. The technique of initiating a discharge by 193 nm laser photo-ionization of TMAE seeded in high-pressure background argon gas that is sustained by inductive coupling of reduced rf power at moderate pressures (<120 Torr) has been demonstrated by Kelly *et al.* [16]. While we have utilized a laser to perform the pre-ionization, a more compact UV flash tube scheme could also be used to initiate the seeded plasma.

The objective of the present work is to investigate the effect of a UV-laser-initiated, axially-extended, high-density seed plasma discharge on the rf-sustained, high-pressure argon or nitrogen plasma through improved rf power coupling and increased rf wave penetration. We also desire to maintain the high density ($10^{11\sim13}$/ cm^3), large volume (~ 1000 cm^3) plasma extending well away from the source region (more than 10 cm) using laser initiation and rf sustainment. A 105 GHz millimeter wave interferometer is employed to determine the line-average plasma density, collision frequency, and electron temperature using a new analysis method. Optical emission spectroscopy is used to characterize the temporal evolution of the plasma. A technique to measure the time-dependent, plasma-loaded antenna impedance $Z_p(t)$, during an rf plasma pulse using a dual rf directional coupler, which can be used for precise capacitive matching to the plasma load, is also presented.

II. Key Aspects of the Research

We have made great strides recently in our research on laser-initiated and radiofrequency-sustained plasmas. High density (10^{11}~ $4x10^{13}$), large volume (500 cc), high-pressure (760 Torr) laser-initiated seed plasmas were produced in nitrogen, argon, and air. These low ionization energy organic gas seed plasmas create an initial condition that can be used for sustainment at much lower radiofrequency (rf) power levels than is the case for radiofrequency initiation alone. We have produced $4x10^{13}$/cc, low temperature (Te<0.3 eV), 500 cc seeded organic gas plasmas with our pulsed 193 nm laser source. Recombination rates and evidence for delayed ionization due to super-excited states were found. When 15 mTorr of the seed gas is mixed with air, nitrogen, argon or helium at 760 Torr, the laser-produced density is in the range of 1-3 x 10^{13}/cc and plasma decay and two- and three-body recombination rates have been measured. By measuring the decay process in pure TMAE (Tetrakis-diMethylAmino-Ethylene) where two-body processes dominate and then adding the high-pressure neutral gas, three-body processes are determined. The use of the laser-produced TMAE seed plasma to provide a load for radiofrequency antenna matching provides a significant reduction in sustainment power compared to high-pressure radiofrequency plasma creation alone. TMAE is compatible with air for up to 10 minutes after introduction and can be readily ionized by UV. Millimeter wave interferometry measurements show that there is a delayed ionization process that results in a peak in the ionization of the seed gas 120 ns after the laser pulse. This process is found to provide a longer density lifetime for the plasma that in air is above $3x10^{12}$/cc for 0.3 μs. This time scale and large plasma volume provides an excellent plasma load for pulsed power rf sustainment.

Highlights of the recent research include:

- Use of UV ionization of low ionization potential seed gas in air to reduce rf power levels for large volume (2500 cc), high density ($10^{12\text{-}13}$/cc) plasmas.

- Development of very precise (ms) computer-controlled timing mechanism for optimum laser firing during the RF power rise to sustain the plasma

- Development of plasma antenna load impedance measurement technique to enable efficient (95%) matching using an electrodeless inductive rf helix for sustained coupling to the plasma.

- First observation and publication of super-excited, laser-produced seed gas states that exhibit delayed ionization and increased lifetime in argon, nitrogen, oxygen and air at densities of $10^{12\text{-}13}/cm^3$ at 760 Torr pressures.

- Contribution to the Diagnostics chapter of a book entitled *Non-equilibrium Air Plasmas* on the topic of new millimeter wave high-pressure plasma diagnostics. We have also contributed, collected, and published material in the book on High Frequency Creation of Air Plasmas, *Non-Equilibrium Air Plasmas at Atmospheric Pressure*, with the PI serving as Chapter Master (126 pages).

- Experiments involving radio frequency sustainment of the laser produced seed plasmas in air, argon and nitrogen, the results of which have been submitted for publication. It was found that higher density plasmas ($>10^{11\text{-}13}$/cc) and larger volumes (>500 cc) can be sustained at a much lower RF power levels and with more enhanced axial projection away from the antenna with laser initiation than without. Power densities of 1-20 W/cc at $10^{11\text{-}13}$/cc in N_2 and Ar at 50 and 760 Torr were obtained using laser initiation versus more than 10 kW/cc initiation and sustainment is required in 760 Torr Air by the usual means.

- Broad spectroscopic (200-1100 nm) measurements of the evolution from the initial TMAE seed plasma to the air, nitrogen or argon high-pressure plasma at 20 Torr later in the RF pulse.

- Radiofrequency creation and measurement of enhanced wave penetration in high density plasmas ($10^{12\text{-}13}$/ cc) in a magnetic field.

III. Characterization of Laser Initiation and Radiofrequency Sustainment of Seeded Air Plasmas at High Pressure

A. Plasma System and Method of Operation

i.) Excimer laser and optic system

A schematic of the experimental setup is shown in Figure 2. A uniform intensity ultraviolet (UV) beam of 193 nm wavelength is produced using an excimer laser (Lumonics Pulsemaster PM-842) that runs in the ArF (6.4 eV per photon) mode. The half-width of the laser pulse is 20 (±2) ns with a 2 ns rise/fall time and a maximum laser energy of 300 mJ. The laser output beam size is rectangular (2.8 cm × 1.2 cm). The laser beam enters a 5.4 cm diameter, 140 cm long Pyrex plasma chamber through a 2.8 cm diameter Suprasil quartz window (98% transparency at 193 nm) at one end. Laser energy passing through the UV window is measured using an energy meter SCIENTECH (Astral AD30). In order to account for the laser attenuation by the UV window, the UV window is placed in front of the energy meter. A laser power flux of 6 mJ /cm^2 is maintained.

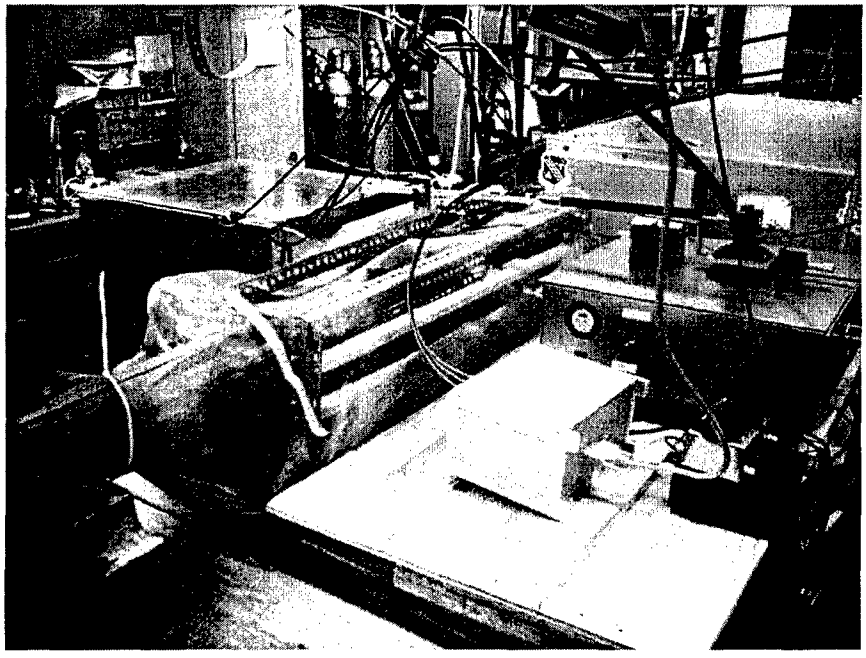

Figure 1. Laser-Initiated, RF Sustained Plasma Experimental Facility

The Figure 2 below illustrates the schematic of the laser initiated, rf sustained plasma facility with the current diagnostics.

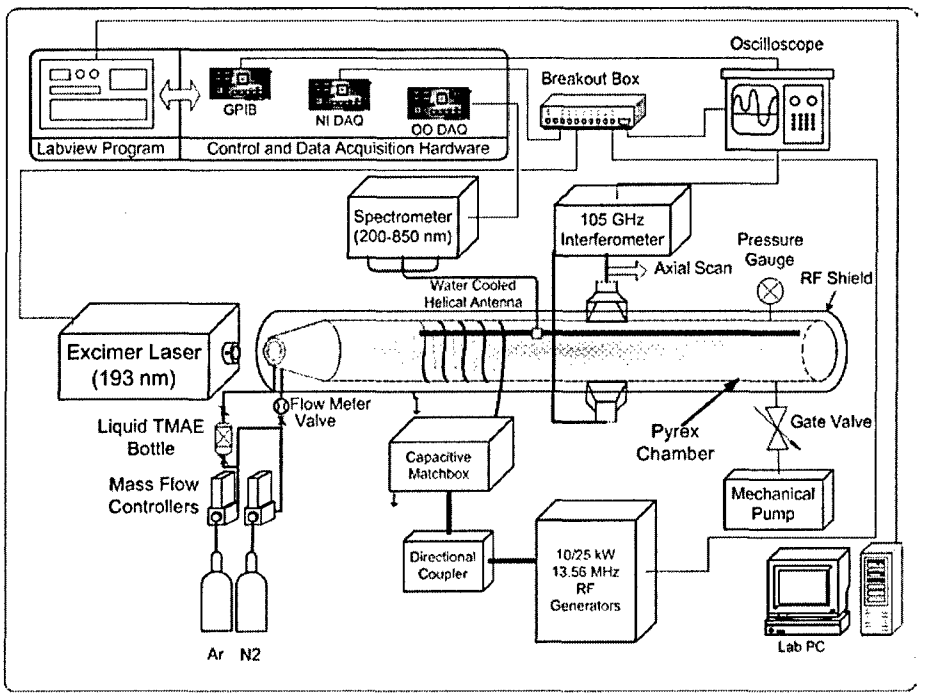

Figure 2. Laser Initiated, RF Sustained Plasma Facility

Figure 3 below illustrates the RF and laser timing pulses as well as the plasma density characteristics during a typical plasma shot. Note that some parts of this figure are expanded in time for clarity.

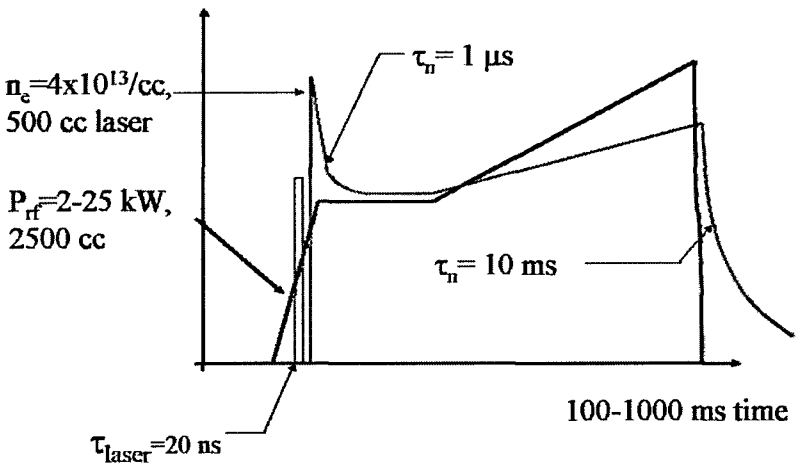

Figure 3. RF, laser and plasma density characteristics during a plasma shot.

Figure 4 below illustrates the plasma density produced in the seed TMAE by the UV laser fluence of 6 mJ/cm^2. It is this plasma that acts as a seed to which the inductive antenna and RF generator must match to couple with reduced RF power densities of 1-10 W/cc at high densities in the 10^{13}/cc in air or other gases.

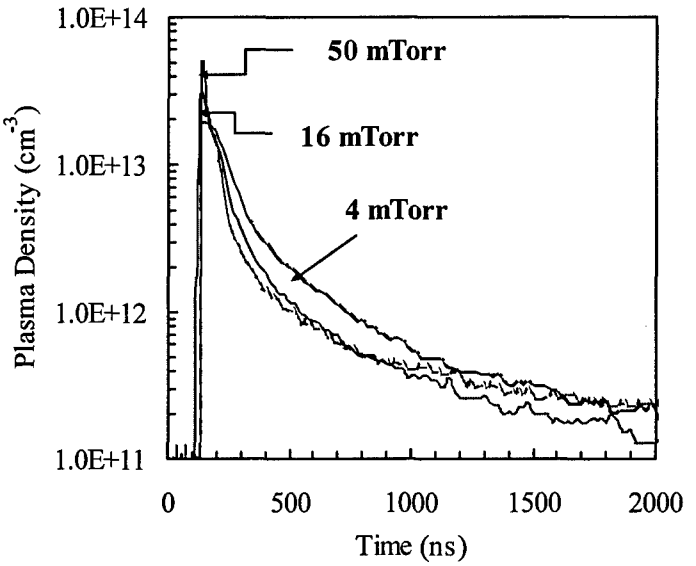

Figure 4. TMAE line-average plasma density Elaser=6.4 eV, Eioniz=6.1 eV at z=20 cm for a laser fluence of 6 mJ/cm^2, τ_L= 20 ns.

ii.) Gas flow system and plasma chamber

Gas mass flow controllers along with a gas injection and mixing system are also located at the laser window end as shown in Figure 2. The 5 cm diameter Pyrex chamber is evacuated to 50 mTorr prior to experiments. After evacuation, a stable chamber pressure is achieved by fine-tuning and balancing the gas input valve and throttle valve of the mechanical pump. A thermal gas flow meter is located at the gas injection pipeline to measure the gas flow rate. A MEMS-based pressure gauge is used to monitor the chamber pressure accurately. Typical gas flow rate ranges from 0.5 standard liters per minute (SLM) to 5.0 SLM, which is related to the chamber pressure level. After a steady chamber pressure and flow rate is established, TMAE is injected into the chamber. Prior to injection, the TMAE cylinder is pressurized with the background gas. For fast injection of TMAE, a quick electro-valve is opened for 1 second time, so that an optimum TMAE gas partial pressure of 15 mTorr [Akhtar, Scharer, Tysk, Denning 2004] is achieved in the chamber.

iii.) RF system: RF source, transmission line matching network and helix antenna

Two radio-frequency generators at 13.56 MHz are available to couple power to the antenna using an efficient capacitive impedance matching network. The first one is a 10 kW solid-state unit (CX10K-S, Comdel, Inc. 13.56 MHz) that is operated in a single pulse mode (τ=100-1000 ms) with very fast (10-5 μs) turn-on/off times. A second unit is a 25 kW solid-state/triode unit (CXH25K, Comdel, Inc.) with variable duty cycle and large (5 kW) fold-back power capacity. The short laser pulse firing (20 ns) is triggered late during the initial rise in the rf power system to provide the seed plasma for efficient rf coupling and sustainment at lower power levels. These two radio frequency sources together provide a broad power range and versatility of operation for the experiment. A dual directional coupler is also used to measure the incident and reflected power. Tektronix high voltage probes located across the two capacitors in the match box allow accurate measurement of the voltage, current and their phase to determine the plasma load impedance $Z_p(t)$, which is a function of time. The rf power is coupled through a helical antenna that excites rf fields in the laser formed plasma. The water-cooled helical antenna is made of 5 turns of quarter-inch copper tube of axial coil length 10 cm and internal diameter 6 cm wound tightly over the 5 cm inner diameter Pyrex plasma chamber. The lower end of the helical antenna is grounded to the capacitive match box that in turn is grounded to the 13.56 MHz RF source. Radio frequency power is coupled to the capacitive impedance matching network using a 1-5/8", 50 Ω semi-rigid coaxial transmission line (Myat Inc.). The capacitive matching network consists of two high-voltage vacuum variable capacitors (GCS-100-7-5S; 5-100 pF, 10 kV, 170 A and CVFP-1000-40S; 35-1000 pF, 40 kV, Jenings Technology) with a series resistance of < 50 mΩ at 13.56 MHz measured using a network analyzer. The match box is enclosed in a conducting box to provide rf shielding. The anticipated lower plasma radiation resistance (1 to 6 ohms) mandates special care required to reduce ohmic losses in the impedance matching network and connections. To reduce rf losses arisng from connection points and solder joints, the antenna has been made out of a continuous length of copper tube with a measured equivalent vacuum series resistance of 0.5 Ω due to contact resistance and skin effect.

iv.) Plasma diagnostic facilities

1.) Quadrature-phase millimeter wave interferometer

A 105 GHz (Quinstar Technology, QBY-1A10UW) quadrature-phase, millimeter wave interferometer is used to characterize the spatial variation and temporal development of plasma electron density and effective collision rate. The interferometer works in the Mach-Zender configuration, in which the plasma is in one arm of the two-beam interferometer (Figure. 5). The principle of plasma interferometery is discussed in section B.-iii of Part III.

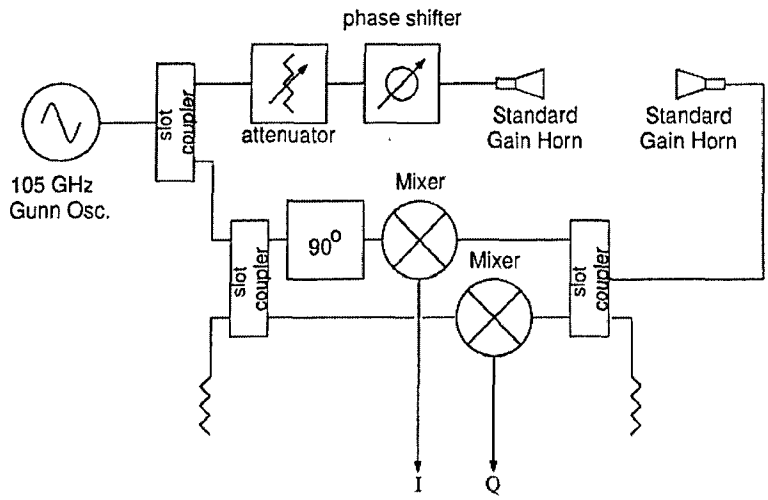

Figure 5. The interferometer of Mach-Zender configuration.

Figure 6 below shows the plasma density as measured by an interferometer when the RF matching system is tuned utilizing the plasma impedance diagnostic measurement to provide a good match (<5 % power reflected) to the laser formed plasma. The laser formed plasma is the initial spike. The RF power can be readily coupled to this seed plasma to sustain the plasma at a much lower power level than would be the case if RF alone were used (1 kW vs 3 kW in this case). In addition, the laser produced seed plasma provides an excellent match for the RF power. This procedure has also been successful in efficiently coupling RF power to nitrogen, oxygen, and air plasmas.

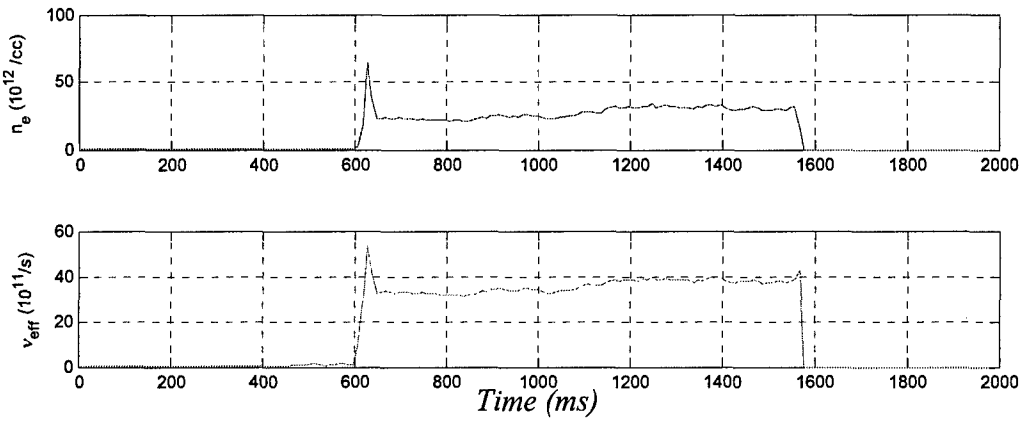

Figure 5. Time dependence of n_e and ν_{eff} in 140 Torr Ar plasma with very efficient RF power coupling during a pulse.

Plasma conditions are Pin=1 kW, $|\Gamma in|^2$=5%; chamber pressure is 140 Torr with 500 cc produced, gas flow rate is 1.5 SLM, and laser power is 100 mJ over 20 ns for seed plasma initiation. The plasma antenna load impedance, Z_L, is found to be 4.3 + j127 Ω using our RF impedance measurement methods.

2.) Plasma impedance measurement facilities

One crucial advance that allows us to create high pressure air constituent plasma is the real-time plasma impedance measurement technique. The plasma impedance is measured *in-situ* and in *real-time* using two methods: method **A** uses a directional coupler, which measures the incident and reflected coupled RF voltage at the input end of the match-box; method **B** employs the two aforementioned high-voltage probes to measure the plasma impedance. A numerical Matlab program solves the plasma impedance based on the two sets of data, and two results are compared and averaged to obtain the actual plasma impedance. The plasma impedance value thus obtained is used to find optimum C_1 and C_2 settings, so that we can further improve the matching and minimize reflected RF power.

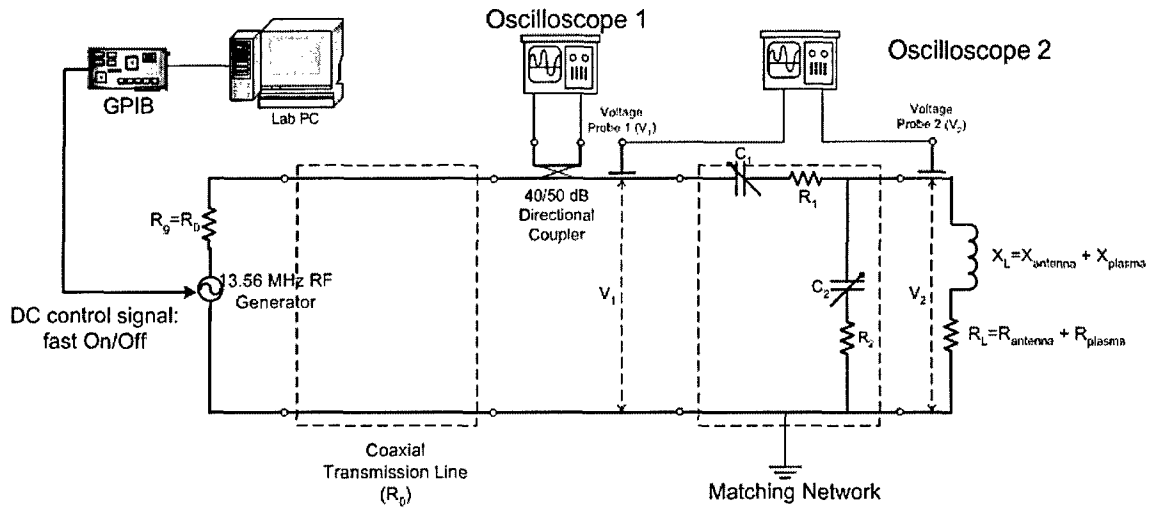

Figure 7. Diagram of the RF circuit.

3. Optical Emission Spectroscopy

Optical emission spectroscopy is used to characterize the temporal evolution of the plasma. The optically emitted spectral lines illustrate the temporal plasma evolution from a TMAE seed plasma initiated by the laser and early RF power to the steady-state RF plasma of neutral background gases such as argon and nitrogen. A three channel, wide band (200 – 850 nm) ST2000 Ocean Optics Spectrometer is used to record the plasma spectral emission perpendicular to the plasma column axis. Each channel is connected to a separate grating spectrometer (1200 lines/mm, with an optical resolution of 0.3 nm), which counts photons using a linear CCD array (2048 pixels). Samples are taken over the following wavelength ranges: 200-500 nm, 400-700 nm, and 600-850 nm. The three channel configuration has three centered blaze wavelength efficiency curves, which provides increased resolution over a single channel model designed for the same wavelength range. The plasma spectral emission collected by a collimating lens is guided through optical fibers and focused on the detectors. The spectrometer output is connected to a PC with an A/D board and the data is acquired using a LabVIEW program developed by our group. The software provides more flexibility in operation and also allows for correction of spectral attenuation of the fiber optics. The

program also controls the triggering of the laser source, the optical system, and the fast digital oscilloscope for data acquisition with accurate timing. The synchronized LabVIEW program triggers the spectrometer to acquire the optical emission at a specified time within the RF pulse, with 50 ms integration time to obtain good signal to noise ratio. By triggering the spectrometer at a specified time, the spectral emission of the early laser initiated seed plasma and later steady-state RF plasma can be obtained, to diagnose the plasma evolution.

4.) Programmable control and automation

A very accurate, computer-controlled timing circuit sequences seed gas injection, laser firing, rf turn-on, and data acquisition. This exact timing sequence is very critical since the rf pulse must be enabled during the laser-formed TMAE plasma lifetime ($\tau \sim 3$ μs) where the seed plasma density is sufficiently large ($n>10^{12}$/cc) to provide sufficient plasma radiation resistance load ($R_p > 1\ \Omega$) for efficient rf coupling.

B. Theoretical Framework

i.) Properties of tetrakis (dimethylamino) ethylene (TMAE) gas

TMAE ($C_{10}H_{24}N_4$), a large molecule, is chosen as seed gas for two reasons: first, the vertical ionization potential of TMAE is 6.1 eV, much lower than that of the background gases; secondly, the TMAE molecule has a large photo-ionization cross-section for ultraviolet radiation and therefore large volume plasmas can be easily created. The continuous UV beamline photo-ionization quantum efficiency of TMAE at 193 nm is 30%. In addition, TMAE is also a strong electron donor. Bright chemiluminescence associated with the reaction of TMAE and air in the gas phase is very long lived and is observable even after 30 min under some conditions. We have also found that the room temperature vapor arising from the liquid form of TMAE is compatible with air over long times and that it is quite viable for efficient laser ionization in air for 10 minutes after introduction. Thus TMAE can be used as a seed gas for air plasma that can be efficiently ionized by a UV laser or a less expensive flashtube.

ii.) Millimeter wave interferometery

Millimeter wave interferometery is used to characterize the spatial variation and temporal development of the plasma [Akhtar, Scharer, Tysk and Denning, 2004]. In low pressure discharges where the wave frequency (ω) is much greater than the plasma frequency (ω_p) and the collision frequency (ν), a linear relationship exists between the plasma density and the phase shift. In this case the wave suffers little or no attenuation as it travels through the plasma. However, at high gas pressures, where the collision frequency is comparable to both plasma and wave frequencies ($\nu \geq \omega \sim \omega_p$), the wave propagating through the plasma arm undergoes phase change as well as strong attenuation. The wave attenuation is caused by the presence of high density as well as high collisionality. In this case the measured plasma density has a complex dependence on wave phase as well as amplitude changes. In order to calculate the refractive and dissipative properties, we consider an electromagnetic wave propagating in an infinite, uniform, collisional plasma. In this model, electron motion is induced by the electromagnetic wave and the ions are assumed to form a stationary background. Even though the laser ionization rate is very large, the assumptions for the model remain valid since the time scale for change in plasma characteristics ($\tau \approx$ 10-100 ns) will be much larger than the wave propagation time through the plasma and the fast response of the detector diode and the oscilloscope ($\tau \approx$ 2 ns). Moreover, most of the density variation and recombination analysis is carried out during the plasma decay in the absence of an ionizing source.

The objective of the plasma interferometry experiment is to accurately diagnose the high pressure plasma over the entire pulse. A new approach has been developed and employed to evaluate the plasma characteristics ν, ω_p, n_e, and T_e, based on the millimeter wave interferometry. Given a plasma with an effective electron-neutral collision rate (ν) and plasma frequency (ω_p), if we launch a plane wave through the plasma, which is assumed to be infinite in dimensions transverse to the direction of microwave propagation and has thickness d along the direction of propagation, the phase constant β_p and attenuation constant α_p of the wave are

[19]:

$$\beta_p = \frac{\omega}{c}\left\{\frac{1}{2}\left(1-\frac{\omega_p^2}{\omega^2+\nu^2}\right)+\right.$$

$$\left.\frac{1}{2}\left[\left(1-\frac{\omega_p^2}{\omega^2+\nu^2}\right)^2+\left(\frac{\omega_p^2}{\omega^2+\nu^2}\frac{\nu}{\omega}\right)^2\right]^{1/2}\right\}^{1/2} \quad (1)$$

$$\alpha_p = \frac{\omega}{c}\left\{-\frac{1}{2}\left(1-\frac{\omega_p^2}{\omega^2+\nu^2}\right)+\right.$$

$$\left.\frac{1}{2}\left[\left(1-\frac{\omega_p^2}{\omega^2+\nu^2}\right)^2+\left(\frac{\omega_p^2}{\omega^2+\nu^2}\frac{\nu}{\omega}\right)^2\right]^{1/2}\right\}^{1/2} \quad (2)$$

Both ν and ω_p are plasma characteristics which are functions of spatial location within the plasma at any given time. They can be written as $\nu\ (z, r, \theta, t)$ and $\omega_p\ (z, r, \theta, t)$, where we use cylindrical coordinates due to chamber geometry. Both ν and ω_p are local characteristics of the plasma. There exist radial as well as axial profiles for plasma density and electron-neutral collision rates. At a given axial location, we assume that the radial density profile is close to uniform. Note that since β_p and α_p are determined by ν and ω_p, they are local values and therefore also have a spatial variation. However, the interferometry method measures the phase shift and attenuation as integration over the entire wave path

$$\Delta\varphi = \int_0^d (\beta_0 - \beta_p)dx \quad (3)$$

$$\Delta A = \int_0^d (\alpha_0 - \alpha_p)dx \quad (4)$$

because the 105 GHz microwave beam penetrates through the entire plasma column and experiences a total phase shift and attenuation. Here, α_0 is the attenuation constant of free

space, β_0 is the phase constant of free space, d is the diameter of plasma chamber and x is the integration variable.

Since it remains impractical to measure the radial profile of v and n_e in an atmospheric-pressure plasma, we assume a 1-D plasma slab model with a radial profile that is approximately uniform due to the high recombination rates. As a result, the integrations in (3) and (4) can be written as:

$$\Delta\varphi = (\beta_0 - \beta_p)d \qquad (5)$$

$$\Delta A = (\alpha_0 - \alpha_p)d \qquad (6)$$

This 1-D uniform plasma slab model is conservative in measuring the peak density and collision rate because it ignores the effect that the chamber wall will have on the plasma and assumes a uniform radial profile of v and ω_p within the plasma. Thus this model calculates a line-average of the plasma density and collision rate over the path the microwave goes through.

In our plasma interferometry experiment, we first measure phase shift $\Delta\varphi$ and attenuation ΔA using interferometer, then use (5) and (6) to calculate the β_p and α_p values, then calculate the plasma characteristics v and ω_p from the calculated β_p and α_p values. Notice that (1) and (2) are explicit expressions of β_p and α_p in terms of v and ω_p. In order to make use of the experimentally measured values for α_p and β_p, it is necessary to invert these equations to produce explicit expressions for v and ω_p. First let us define two intermediate variables X and Y given by

$$X = \frac{1}{2}\left(1 - \frac{\omega_p^2}{\omega^2 + v^2}\right) \qquad (7)$$

$$Y = \frac{1}{2}\left[\left(1-\frac{\omega_p^2}{\omega^2+v^2}\right)^2+\left(\frac{\omega_p^2}{\omega^2+v^2}\frac{v}{\omega}\right)^2\right]^{1/2}$$

$$=\frac{1}{2}\left[(2X)^2+\left(\frac{\omega_p^2}{\omega^2+v^2}\frac{v}{\omega}\right)^2\right]^{1/2} \qquad (8)$$

By substituting X and Y into (1) and (2), β_p and α_p can be simplified as (9) and (10):

$$\beta_p = \frac{\omega}{c}\{X+Y\}^{1/2} \qquad (9)$$

$$\alpha_p = \frac{\omega}{c}\{-X+Y\}^{1/2} \qquad (10)$$

We can solve (9) and (10) for X and Y in terms of β_p and α_p:

$$X = \frac{c^2}{2\omega^2}\left(\beta_p{}^2-\alpha_p{}^2\right) \qquad (11)$$

$$Y = \frac{c^2}{2\omega^2}\left(\beta_p{}^2+\alpha_p{}^2\right) \qquad (12)$$

By inverting (7) and (8), we can calculate v as

$$v=2\omega\frac{\left(Y^2-X^2\right)^{1/2}}{(1-2X)} \qquad (13)$$

and ω_p as

$$\omega_p = \left[(1-2X)\left(\omega^2+v^2\right)\right]^{1/2} \qquad (14)$$

So ultimately, we can write v and ω_p in terms of the experimentally measured values β_p and α by plugging the expression of X and Y in (11) and (12) into (13) and (14):

$$v=2\left(\frac{c^2}{\omega}\right)\left[\frac{\alpha_p\beta_p}{1-\frac{c^2}{\omega^2}\left(\beta_p{}^2-\alpha_p{}^2\right)}\right] \qquad (15)$$

$$\omega_p = \left\{ \left[1 - \frac{c^2}{\omega^2}\left(\beta_p{}^2 - \alpha_p{}^2\right) \right] \times \right.$$

$$\left. \left[\omega^2 + 4\left(\frac{c^4}{\omega^2}\right)\left(\frac{\alpha_p \beta_p}{1 - \frac{c^2}{\omega^2}\left(\beta_p{}^2 - \alpha_p{}^2\right)} \right)^2 \right]^{1/2} \right\} \qquad (16)$$

The plasma frequency is related to electron density (cm^{-3}) by:

$$\omega_p = 2\pi \times 8.98 \times 10^3 \sqrt{n_e} \qquad (17)$$

so we can calculate n_e from ω_p. (15) and (16) are inversions of (1) and (2). They are explicit and exact expressions of ω_p and ν with all the right-hand side terms known or measurable from interferometer. Expressions for these quantities were derived in an earlier work [19] using approximations for highly and weakly collisional cases. Since neither of these approximations is valid in the present experiment, it is necessary to use the exact expressions we have derived here.

In addition to characterization of ω_p, n_e, and ν, we have developed an average electron temperature (T_e) diagnostic using plasma interferometry based on the equation for the dominant electron-neutral collisions [20]:

$$\nu = \sigma(T_e) n_0 \overline{|v|} \qquad (18)$$

in which $\sigma(T_e)$ is the total collision cross-section of the collision processes between electrons and neutrals, n_0 is the neutral density, and $\overline{|v|}$ is the average magnitude of the velocity of the electrons. Note that the total cross section σ is a function of T_e. The curves illustrating this dependence in various gases are summarized by Zecca and Shkarofsky [21], [22]. The total cross section curves generalized by Zecca *et al.* are used. We used 4th order polynomial functions to fit these experimental cross section data curves and obtain $\sigma(T_e)$ for use in (18).

The neutral density n_0 is obtainable from the ideal gas law

$$p=n_o RT_g \qquad (19)$$

where p is the neutral gas pressure, n_o is the neutral density, and T_g is the global neutral gas temperature as opposed to the local neutral gas temperature within the plasma (T_l). It is necessary to draw a distinction between the global neutral gas temperature and local neutral gas temperature because due to electron heating of the neutral gas, the local neutral gas temperature will increase significantly after plasma formation inside the helical antenna where T_e is shown to be on the order of magnitude of 1 eV. Neutral density is thus $n_o = p/(RT_g)$. The initial T_g that exists before the laser or rf is pulsed is useful for determining the overall neutral density because the neutral gas molecules are contained in the chamber during the plasma pulse with very negligible escape from the chamber due to gas heating and pumping.

If we assume a three-dimensional Maxwellian velocity distribution for the electrons, the average velocity of electrons $\overline{|v|}$, is related to electron temperature T_e by [20]:

$$\overline{|v|} = \left(\frac{8k_B T_e}{\pi m_e}\right)^{1/2} \qquad (20)$$

where k_B is the Boltzmann's constant and m_e is the electron mass. We rewrite (18) as $\overline{|v|} = \nu/\left(\sigma(T_e)n_0\right)$, and plug it into the right hand side of (20) to obtain:

$$\frac{\nu}{\sigma(T_e)n_0} = \left(\frac{8k_B T_e}{\pi m_e}\right)^{1/2} \qquad (21)$$

in which T_e is the only unknown because the collision rate ν is measurable from the interferometry data, n_0 is obtainable from (19), and $\sigma(T_e)$ is documented [21] and [22]. Notice that T_e is on both sides of (21), which means that an iterative root-finding routine is needed to solve for T_e using this method. The interferometer and method of analysis was previously compared [23] with a Langmuir probe to obtain line-average density measurements in a lower pressure helicon plasma source over a wide range of densities and magnetic fields. The two measurements were found to be in agreement within 8% over a density range from $4 \times 10^{12}/\text{cm}^3$ to $1.5 \times 10^{13}/\text{cm}^3$. No approximation is used to derive (15), (16) and (21), so they are

exact solutions of v, ω_p and T_e which can be used to calculate temporal variation of the plasma characteristics during each plasma pulse as well as the average value over the pulse. They are thus applicable to wide range of experiments in which interferometry is available. Axial profiles of the plasma characteristics can also be obtained using this method.

iii.) Plasma impedance measurement

One important advance that allows us to create fast, pulsed, high-pressure plasmas with lower rf power levels is a real-time plasma impedance measurement technique that we have developed that allows efficient matching of the 50 Ω rf network to the time varying plasma load. We define the plasma-loaded helical antenna radiation impedance Zp(t)= Rp(t)+ jXp(t) (also referred to simply as the plasma impedance) as the impedance measured at the input to the antenna feeds from the capacitive matchbox. This impedance is a function not only of the character of the helix itself, but also of the plasma initiated by the laser and sustained by the rf pulse. We write Zp(t) as a function of time *t,* meaning the rf load is a function of time during the whole laser initiation and rf sustainment sequence. Before the 20-ns laser pulse breaks down the TMAE seed plasma, the chamber is filled with neutral gas that behaves essentially like a vacuum (μ_0, ε_0). Immediately after the laser pulse and the 100 ns delayed ionization process [15], [17], the plasma is formed in the chamber and sustained by the rf power. During this time the laser pulse can lead to high-pressure plasma fluctuations that are observed visually by photography. The dielectric properties of the plasma are substantially different from the vacuum antenna load. The permittivity of the plasma depends on ne and ν of the plasma, both of which vary substantially during the rf sustainment period due to transient behavior of the high-pressure plasma. As a result, the rf load Zp(t) will exhibit a very fast transition when the plasma is initiated by the laser and varies in time due to the high-pressure plasma fluctuations and plasma recombination processes. It is of considerable interest to obtain Zp(t) because the knowledge of plasma impedance provides the information that allows us to tune the capacitors for optimal rf matching during the rf pulse. This is crucial to achieve a high rf power coupling efficiency rapidly in a pulsed plasma and to protect the high

power rf generator from reflected power. Optimal matching can reduce the rf power levels, weight, and cost requirements for making pulsed high-pressure plasmas by measuring the rf load impedance in real-time to enable good matching of the final-stage steady-state plasma load to the 50 Ω rf impedance network.

We measure the plasma impedance in-situ and in real-time using a dual directional coupler. The incident and reflected voltages (Vin and Vref) are measured by the coupler connected to the oscilloscope (as in the rf circuit diagram shown in Fig. 7) so that the input reflection coefficient Γin is found as Γin=Vrfl / Vinc. Zin, the input impedance looking into the match box, is calculated as Zin(t) = Z0 (1 + Γin(t)) / (1 - Γin (t)). Zp(t) is thus:

$$Z_p(t)=\frac{Z_2\left(Z_{in}(t)-Z_1\right)}{Z_1+Z_2-Z_{in}(t)} \quad (22)$$

in which Z1 and Z2 are the impedances of the tunable capacitors C1 and C2, characterized by network analyzer measurements. A Matlab program solves for the plasma impedances based on the Vin and Vref data grabbed by the oscilloscope. The plasma impedance value after the rf sustainment condition is obtained is used to determine the optimum C1 and C2 settings, so that we substantially improve the impedance matching and minimize reflected rf power for subsequent pulses. This is thus an iterative procedure, in which first the two capacitors are set to some neutral position so that a plasma can be formed by laser initiation and rf sustainment. Then a laser/rf pulse is applied using the desired plasma conditions including gas pressure, gas flow and rf power level from which a data set from the directional coupler is obtained. Although a plasma may form, a mismatch may occur resulting in as high as 40% rf power reflection. With the Vinc(t) and Vrfl(t) data obtained, (22) can be used to calculate antenna radiation impedance Zp(t). With Zp(t).calculated for this run, we can calculate the optimum C1 and C2 for the plasma sustained by rf and tune the capacitors accordingly for subsequent experimental runs. The result is very satisfactory. For 760 Torr argon plasma, we are able to reduce the rf power reflection coefficient (|Γ|2) to 10-20%, and for a 50 Torr nitrogen plasma, |Γ|2 is reduced to 5% for the final rf sustainment stage of the plasma. The reason that reflections cannot be reduced below 10-20% for 760 Torr argon plasma is that the argon plasma resistance experiences a large change from 0.5 to 5 Ω as the steady-state plasma is

formed. Due to this large change in plasma impedance, it is not possible to tune for a perfect match for the final steady-state plasma impedance because if this is done, the mismatch at the initiation of rf power will be too great. This mismatch makes it impossible for the rf plasma to form and causes a high level of power reflection, endangering the rf generator. For the 50 Torr nitrogen plasma experiment, due to a smaller change (from 0.5 to approximately 2 Ω) in resistive impedance, we can achieve a better matching with only a 5% rf power reflection coefficient.

C. Experimental Results and Discussion

We first supply the chamber with steady background gas (argon or nitrogen) flow to maintain the desired chamber pressure. Then we inject 15 mTorr of seed TMAE gas mixed with the chamber gas (argon or nitrogen) into the chamber seconds prior to each experiment. The TMAE seed plasma is initiated by a 20 ns UV laser pulse generated by the excimer laser [15], [17] and sustained by the rf generator, which is typically set to provide between 1 and 6 kW of net coupled power. The plasma is diagnosed to determine the electron number density (ne) and effective electron-neutral collision rate (ν) using the 105 GHz interferometer. The electron temperature (Te) is determined based on the effective electron-neutral collision rate and the documented total electron-neutral collision cross section data for Ar. The plasma impedance is measured by analyzing the incident and reflected voltage using the dual directional coupler and the voltages across the two capacitors in the match box using the high-voltage probes.

i.) Optical Emission Measurements

The temporal evolution of argon plasma from the TMAE seed plasma is shown in Fig. 8(a) through (c). In this set of measurements 15 mTorr of TMAE seed gas is mixed with 760 Torr of argon with a gas flow rate of 4.5 SLM. The TMAE seed plasma is produced by laser pre-ionization followed by 2.5 kW of net RF power is coupled to the seed plasma to produce the steady-state argon plasma. The spectrometer is triggered to capture the broad (200-800 nm) spectrum at three different times during the 1 second RF pulse with an integration time of 50 ms.

The captured spectrums are shown in Fig 8 a)- (c) which illustrate the transition from the

TMAE seed plasma to the argon steady-state plasma. Fig 6 (a) shows the shows the broad emission spectrum of the complex TMAE seed gas molecule at t = 50 ms. The seed plasma dominates the entire spectrum early in the pulse. Fig 6 (b) shows that at t = 200 ms the argon lines begin to dominate the spectrum. At t = 400 ms as shown in Fig 6 (c) the steady-state argon plasma is reached with negligible seed gas presence. Thus the laser ionization of the TMAE seed gas and transition to argon plasma is readily accomplished with our system. The evolution in a 50 Torr nitrogen plasma is very similar, and is shown in Fig 9 a)-(c), which show the plasma emission at 50, 100, and 300 ms after the laser pulse.

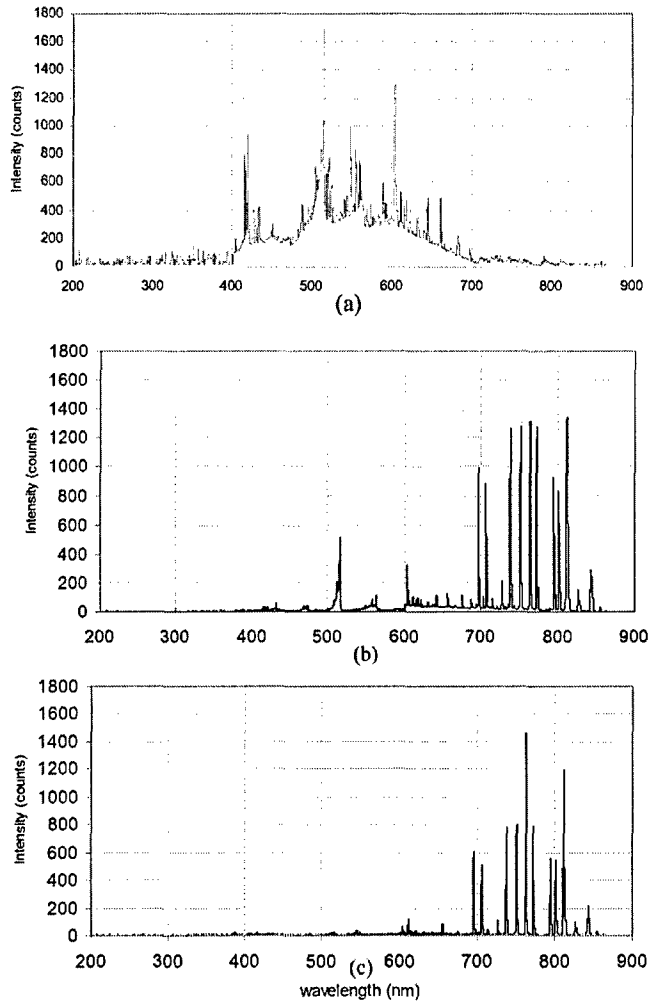

Fig. 8 Temporal evolution of early TMAE seed plasma and later steady-state RF argon plasma emission spectrum: (a). t = 50 ms; (b). t = 200 ms; (c). t = 400 ms. Net RF power of 3 kW, 5 mTorr TMAE and 50 Torr argon, integration time 50 ms.

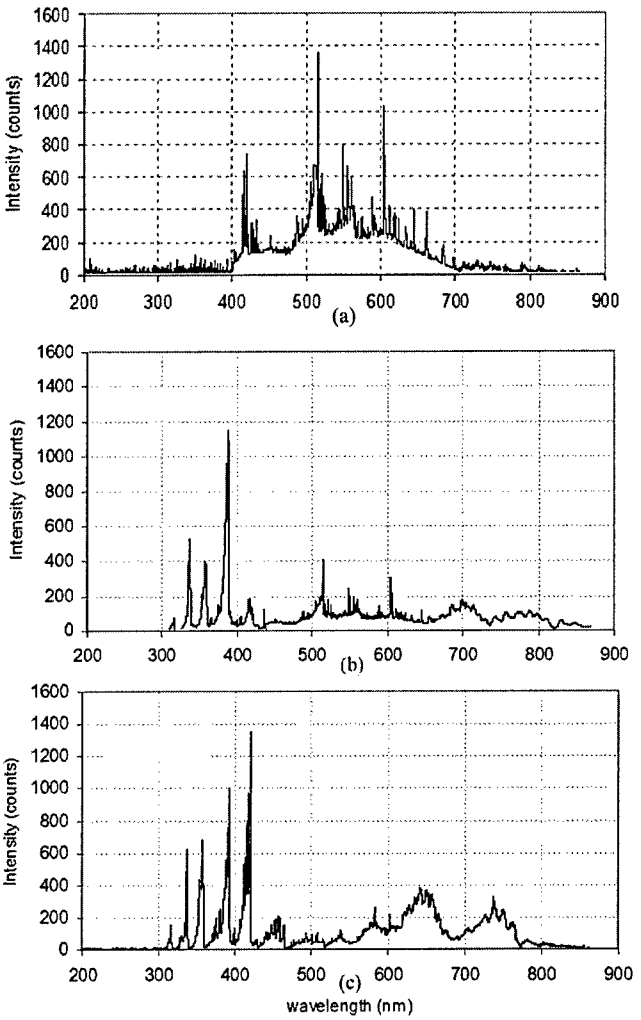

Fig. 9 Temporal evolution of early TMAE seed plasma and later steady-state RF nitrogen plasma emission spectrum: (a). t = 50 ms; (b). t = 100 ms; (c). t = 300 ms. Net RF power of 3 kW, 5 mTorr TMAE and 50 Torr nitrogen, integration time 50 ms.

ii.) Argon Plasma

In a typical pulsed argon plasma sequence, 2.5 kW of net rf power is used in conjunction

with the 100 mJ laser pulse and 15 mTorr TMAE seed gas to initiate and sustain the plasma. The gas pressure of argon is 760 Torr which is maintained by 4.5 SLM flow rate. The valve of the mechanical pump is carefully set to balance the input gas and provide a steady chamber pressure of 760 Torr. Temporal as well axial variation of plasma characteristics are diagnosed and presented in this section.

1) Time-Resolved Electron Number Density, Effective Electron-Neutral Collision Rate, and Electron Temperature Measurements in Argon: It is observed that the laser-initiated, rf-sustained, TMAE-seeded argon 760 Torr plasma goes through two distinct stages. The rf power is initiated at t = -210 ms and the laser pulse is triggered when the incident rf power output reaches approximately 90% of the maximum value (at t = 50 ms). Note that since we set the oscilloscope to trigger at the initial laser power supply charging, the laser actually fires at t = 50 ms because it requires a 50 ms charging delay before firing. In other words, the rf power ramps up to 90% of its maximum power 260 ms after the rf pulse is triggered, at which time the laser is fired to form the initial seed plasma. The 20 ns laser pulse produces a high density plasma [15], [17] with ne=$5x10^{12}$-10^{13}/ cm^3 with a 2.8×1.2 cm^2 foot print that is observable on the interferometer with a decay on the μs time scale. Immediately after the laser plasma pulse is formed, a narrow plasma is formed under the antenna that fluctuates spatially, as shown photographically in Fig. 10.

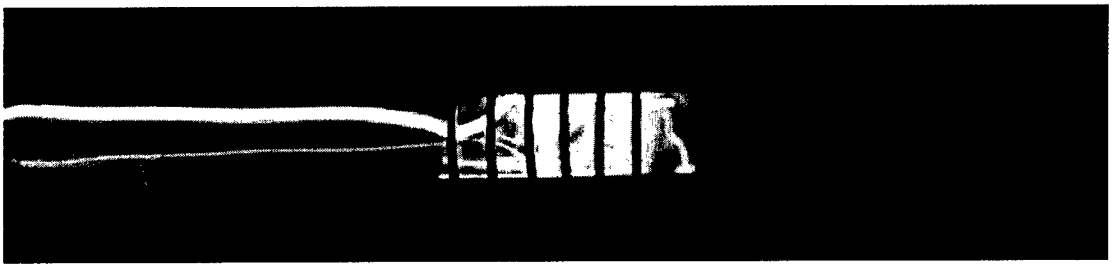

Fig. 10 Intermediate formation stage of the argon plasma. 760 Torr neutral pressure is maintained by 4.5 SLM argon gas flow. 100 mJ laser energy and 2.5 kW net rf power is used to initiate and sustain the plasma.

This is the intermediate formation stage of the plasma. During a typical rf pulse, this stage lasts for 133 ms. The fluctuating nature of the plasma during this stage precludes

measurement using the interferometer. At t = 183 ms (133 ms after the laser pulse), the plasma evolves into a stable, high-density, large-volume argon plasma (Fig. 12) which is readily diagnosed by the interferometer. It is important to note that without the laser initiation pulse, the plasma cannot be initiated nor sustained with comparable power levels at these pressures. On the rf power figures (Fig. 11 (a) and (b)), a sharp fall in the rf power reflection coefficient is observed, corresponding to the formation of the second stage plasma.

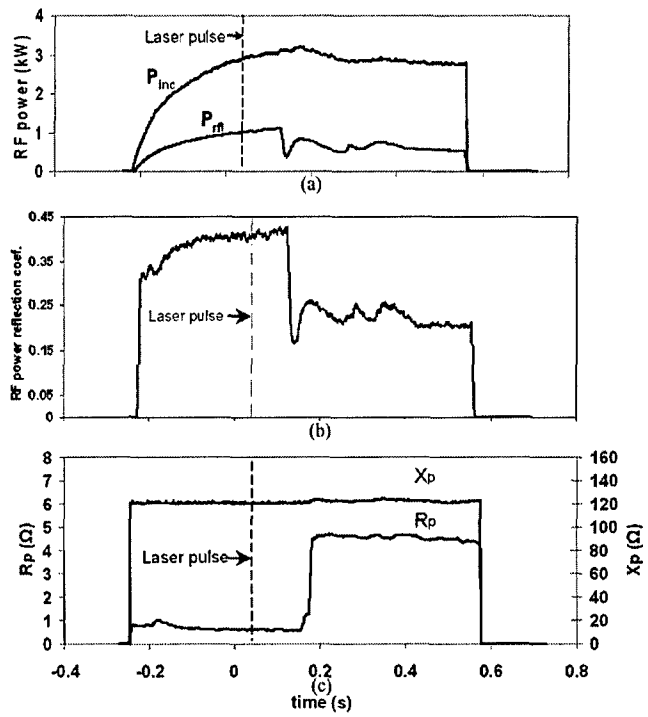

Fig. 11. (a). Incident and reflected RF power over a typical pulsed laser and rf generated argon plasma sequence; (b). Temporal variation of rf power reflection coefficient over the pulsed argon plasma sequence; (c). Temporal variation of R_p and X_p of this pulsed argon plasma sequence.

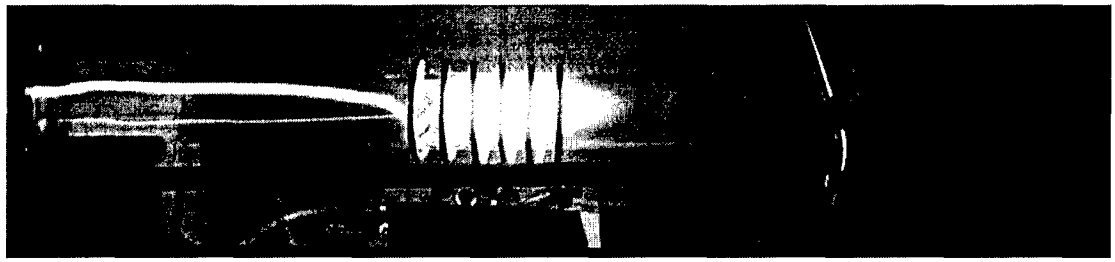

Fig. 12. Steady-state stage of argon plasma. Same conditions as Fig. 3.

The 5 cm line-average electron density, effective electron collision rate and electron temperature is diagnosable using the interferometer after the second stage of plasma (steady-state plasma) is formed. The two signals (in-phase and quadrature-phase) from the interferometer are acquired by two channels of the oscilloscope, which are used to extract the phase shift and attenuation of the wave after it penetrates the plasma [18], [19]. A raw interferometer trace in X-Y mode is presented in Fig. 13.

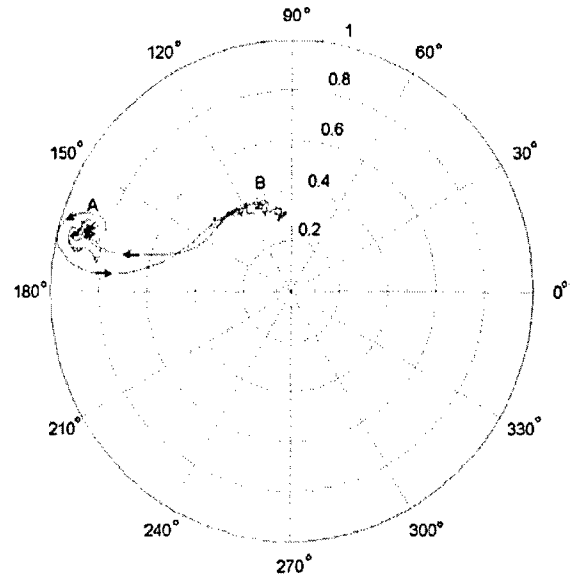

Fig. 13. Interferometer trace of a typical laser plus rf plasma sequence. 760 Torr neutral pressure is maintained by 4.5 SLM argon gas flow. 100 mJ excimer laser energy and 2.5 kW net rf power is used to initiate and sustain the plasma.

Point A corresponds to the vacuum case when the plasma is not present. Point B corresponds to the steady-state plasma condition created by laser initiation and rf sustainment with delayed phase and dampened amplitude compared with A. The trace makes a transition from point A to B when the steady-state plasma is formed at t=133 ms, then back to A when the rf power is turned off at t =575 ms. Using the previously discussed mathematical method, the time-resolved ne, ν and Te are calculated and presented in the Fig. 14 (a) through (c). The resulting 5 cm diameter, line-average electron density, electron collision rate, and electron temperature for the argon case are: ne= 4.5×10^{12} cm^{-3}, ν = 1.1×10^{11} Hz and Te =1.3 eV. Even under steady-state conditions, we still observe some fluctuation in these measurements due to fluctuations in high-pressure plasmas [6].

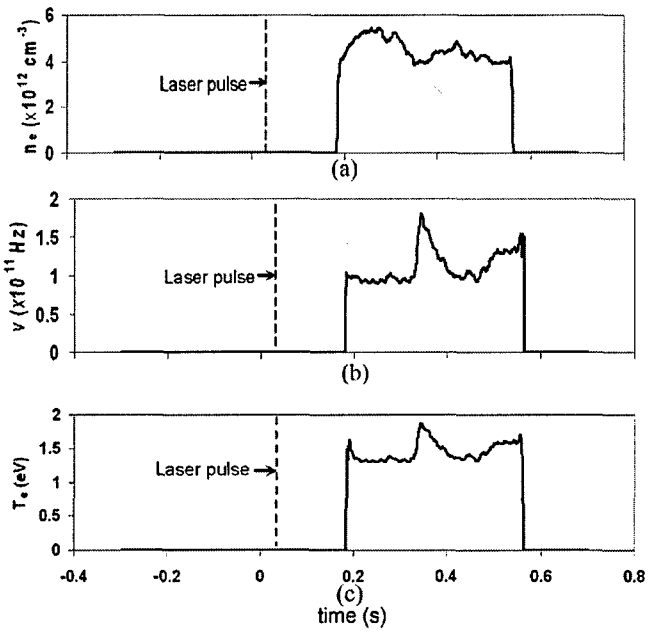

Fig. 14. (a). Temporal variation of electron density of the pulsed argon plasma sequence; (b). Temporal variation of effective electron-neutral collision rate of the pulsed argon plasma; (c). Temporal variation of the electron temperature of the pulsed argon plasma.

2) Plasma Impedance Measurements in Argon: One important aspect of rf sustainment of the laser initiated plasma is to ensure that the rf matching is very good over the majority of the pulse, so that high rf power coupling efficiency can be achieved and the rf generator can be protected from high levels of reflected power. In order to achieve good matching, the rf temporal impedance variation is measured over the rf pulse and the plasma-loaded antenna impedance Zp(t)=Rp(t)+jXp(t) is obtained as shown in Fig. 11 (c). It is observed that Rp, the resistive load, exhibits a transition from 0.5 Ω to 5 Ω when the steady-state plasma is formed, while the inductive load Xp(t) shows a very small increase. This change in load resistance means we have to deal with two very different plasma load impedance levels during the pulse. We typically set the matching network to match the impedance of the steady-state plasma Z_p (5 + j120 Ω) to 50 Ω, and allow a higher reflection level at the beginning of the pulse (which the rf generator can accept because of its high foldback tolerance of 5 kW). As a result, we obtain ≤ 20% rf power reflection during the steady-state plasma.

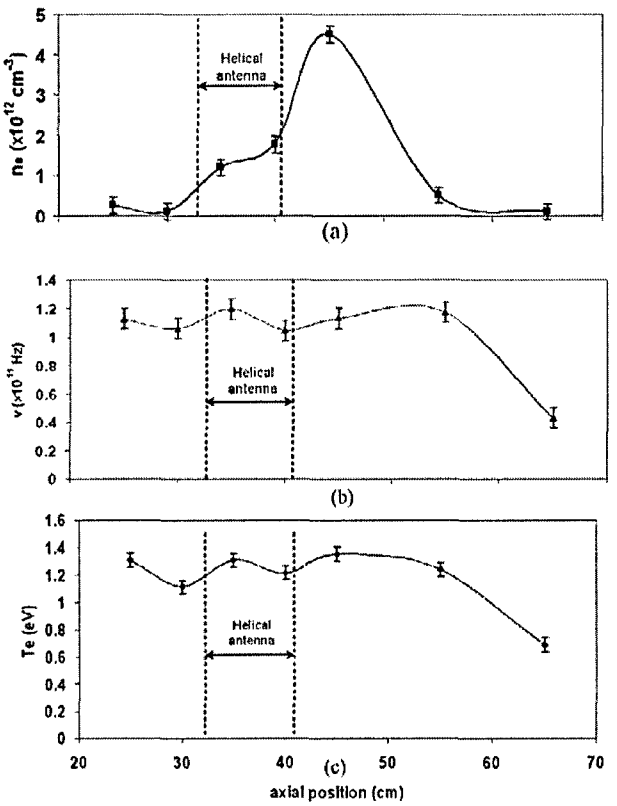

Fig. 15. Axial profile of plasma characteristics of the argon plasma: (a). electron density; (b). effective electron-neutral collision rate; (c) electron temperature. The two dashed lines mark the position of two ends of the helical rf antenna.

3) Axial Variations of Density, Collision Rate and Electron Temperature in Argon: The axial profile of the line-average plasma characteristics ne, ν and Te are also diagnosed and presented in Fig. 15. As shown in the figures, we have achieved a high pressure argon plasma that extends axially from the helical antenna. The peak density occurs about 4 cm downstream from the helical antenna and the plasma extends approximately 20 cm beyond the antenna. The axial profiles of ν and Te are relatively flat.

Significant reduction in rf power levels required to sustain large volume high-pressure argon discharges was achieved compared to that required for rf only plasma initiation and sustainment. The steady-state rf power density required for the sustainment of the argon plasma is 5.0 W/cm^3 at an electron density of 4.5×10^{12}/cm^3 at 760 Torr. The seed plasma also provides a good load for efficient rf coupling at lower power levels via pulsed inductively coupled sources.

iii.) Nitrogen Plasma

A similar method is used for the nitrogen case as for the argon plasma experiment. In a typical pulsed plasma sequence, 5.5 kW of net rf power is used in conjunction with the 100 mJ laser pulse and 15 mTorr TMAE seed gas to initiate and sustain the nitrogen plasma. The nitrogen gas pressure is 50 Torr, maintained by 1.5 SLM flow rate.

1) Time-Resolved Electron Number Density, Effective Electron-Neutral Collision Rate, and Electron Temperature Measurements in Nitrogen: The nitrogen plasma exhibits a lower electron density of 3.5 x 10^{11}/cm^3, but similar levels of $\nu\sim1.4\text{x}10^{11}$/s and Te=1.0 eV (Fig. 17) when compared with the argon plasma. As shown in Fig. 17 and 18, the duration of the intermediate formation stage is approximately 50 ms, much less than that of argon: the rf power is turned on at t=-70 ms, the laser is fired at t=50 ms, then the steady-state nitrogen plasma is formed at t=100 ms. The steady-state nitrogen plasma which occurs 50 ms after laser firing has strong a visible light emission (Fig. 16).

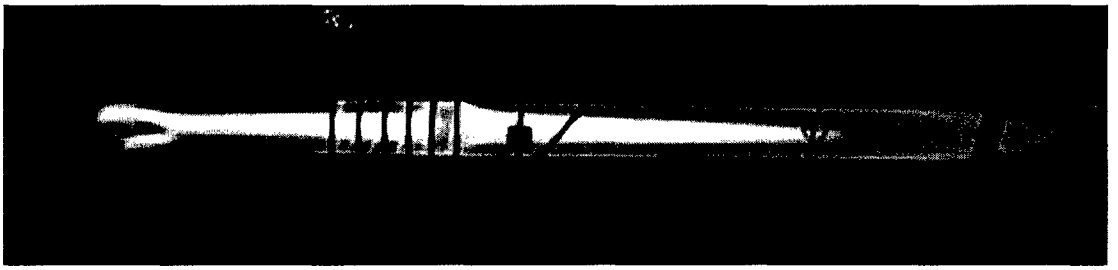

Fig. 16. Steady-state stage of nitrogen plasma. 50 Torr neutral pressure is maintained by 1.5 SLM argon gas flow. 100 mJ excimer laser energy and 5.5 kW net rf power is used to initiate and sustain the plasma.

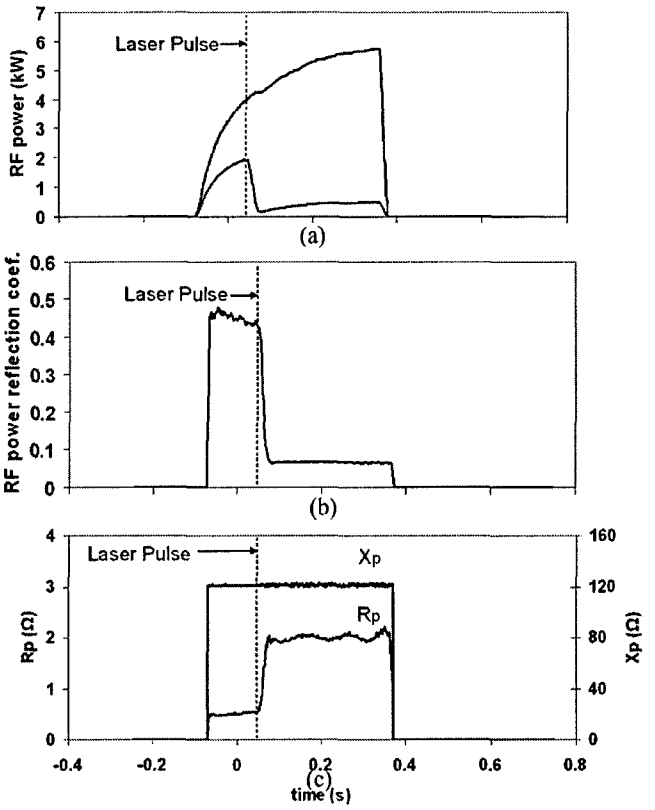

Fig. 17. (a). Incident and reflected RF power over a typical pulsed laser and rf generated nitrogen plasma sequence; (b). Temporal variation of rf power reflection coefficient over the pulsed argon plasma sequence; (c). Temporal variation of R_p and X_p of this pulsed argon plasma sequence.

It has a very bright purple core surrounded by dimmer blue peripheral region. The intermediate formation stage of this 50 Torr nitrogen plasma is much shorter than the 760 Torr argon plasma. The much reduced intermediate stage is the result of operation at lower neutral pressure. The single-photon 193 nm excimer laser direct and delayed ionization substantially enhances the rf penetration away from the helical antenna. If only rf power is used to initiate and sustain the nitrogen plasma, it is only possible to make a plasma at lower than 10 Torr nitrogen neutral pressure, and this plasma is present only under the helical antenna. The laser initiation technique is crucial for reducing the rf power required to sustain the large-volume nitrogen plasma: a power density of 5.5 kW/cm^3 is sufficient to sustain a nitrogen plasma of density 1. 4 × 10^{11}/cm^3 at 50 Torr with laser initiation.

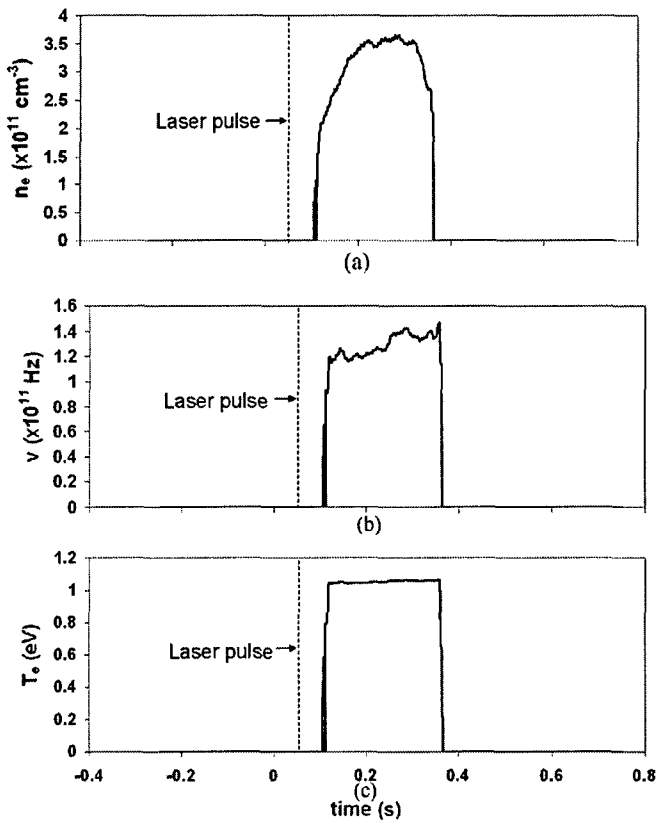

Fig. 18. (a). Temporal variation of electron density of the pulsed nitrogen plasma sequence; (b). Temporal variation of effective electron-neutral collision rate of the pulsed argon plasma; (c). Temporal variation of the electron temperature of the pulsed argon plasma.

2) Plasma Impedance Measurements in Nitrogen: Generally, the nitrogen plasmas show much less fluctuation in plasma characteristics than argon plasma, which is also attributed to lower neutral pressure operation. The transition in resistive plasma impedance from the intermediate to steady-state conditions also occurs for the nitrogen plasma, but it is of lower magnitude due to the lower plasma density when compared to the argon plasma: the resistive load increases from vacuum level of 0.5 Ω to 2.1 Ω when the steady-state plasma is formed. This results in a better rf power coupling efficiency for the nitrogen plasma. A remarkably low rf power reflection coefficient of 5% is achieved for the steady-state nitrogen rf plasma when we use the tuning procedure.

3) Axial Variations of Density, Collision Rate and Electron Temperature in Nitrogen: The line average axial profiles of ne, ν and Te are presented in Fig. 19. The nitrogen plasma density also exhibits a bell-shaped axial profile. The high density plasma region extends 40 cm from the end of the helix along the z-axis as measured by the interferometer, although visually it is observed occupying the whole 1m long chamber.

Earlier, research by Eckert et al [11] on a much higher rf power (22-35 kW) argon and air plasma source was tuned over minutes from a start-up at 1 Torr to 760 Torr. They used the N2 second positive line ratio spectroscopic diagnostic to obtain an electron temperature of Te=0.61 eV for 760 Torr air. In more recent research by Laux [24] on a 50 kW rf plasma source utilizing several spectroscopic techniques and a computer code obtained electron temperatures of 0.64 eV in 760 Torr air. Our interferometer diagnostic technique yields an electron temperature of 1.3 eV in argon at 760 Torr and 1.0 eV in nitrogen at 50 Torr. Our experiment differs from these in that the plasma is formed much faster and with lower rf power, and with a different plasma diameter (larger than Laux's experiment, smaller than Eckert's experiment). The electron temperatures obtained in our case are expected to be somewhat higher for 760 Torr argon and 50 Torr nitrogen. Thus the values obtained are consistent with these other measurements of high pressure rf plasma sources.

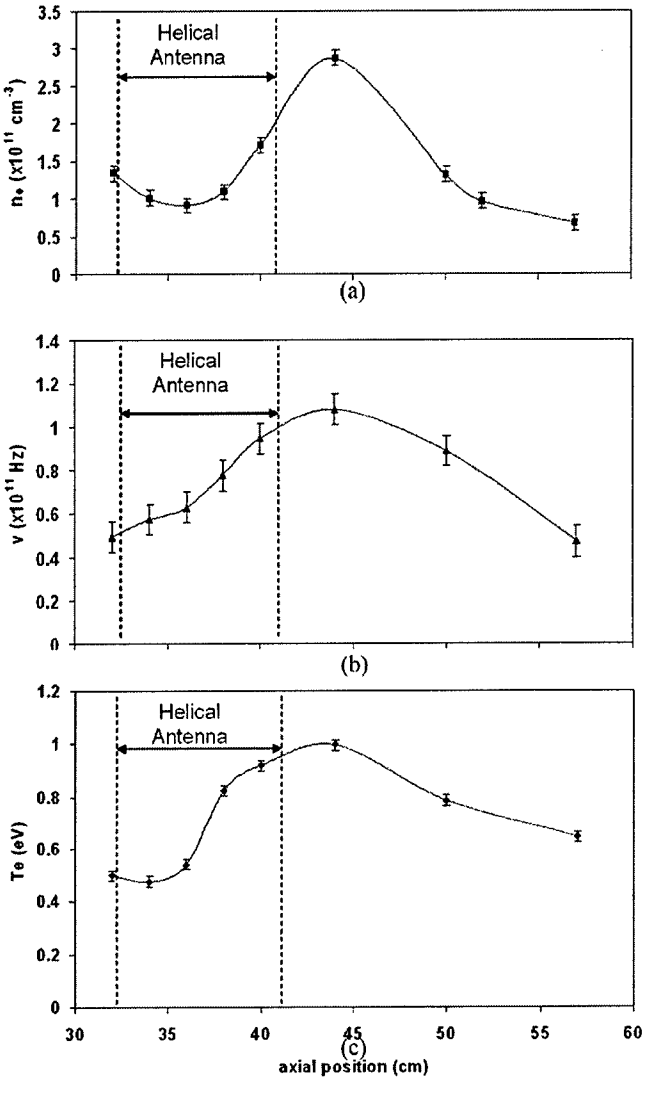

Fig. 19. Axial profile of plasma characteristics of the nitrogen plasma: (a). electron density; (b). effective electron-neutral collision rate; (c) electron temperature.

IV. Helicon Plasma Facility for Radiofrequency Power Penetration in Magnetized Plasma Sources

We have conducted experiments on a magnetized helicon plasma utilizing argon, helium, and deuterium. The setup consists of a 2-m-long, 10-cm-diameter pyrex chamber that is brought down to a vacuum base pressure of 1 x 10^{-7} Torr. Five electromagnets provide an axial static magnetic field of up to 1 kG. Radiofrequency power is coupled into the plasma through a half-turn double helix with pulsed power of up to 3 kW available. Gas is fed upstream from the pumps to provide gas flow which enhances the axial extent of the plasma and provides neutrals for ionization, in contrast to schemes that rely on diffusion of the gas to the antenna region that can result in neutral starvation. Plasmas are produced in argon, helium, and deuterium. A number of diagnostics are available to characterize the plasma. A cylindrical Langmuir probe measures the electron temperature and density. The plasma density is also measured with a 105-GHz ineterferometer that measures the line-average density across the 10 cm diameter. A wave magnetic "B-dot" probe consisting of a small (2 mm diameter), glass-enclosed five-turn coil oriented along the axis of the experiment allows measurement of the wave B_z component. The optical emission can also be observed with a 0.5 m focal length monochromator and can be phase-correlated to the input rf by binning the photomultiplier tube signal via software.

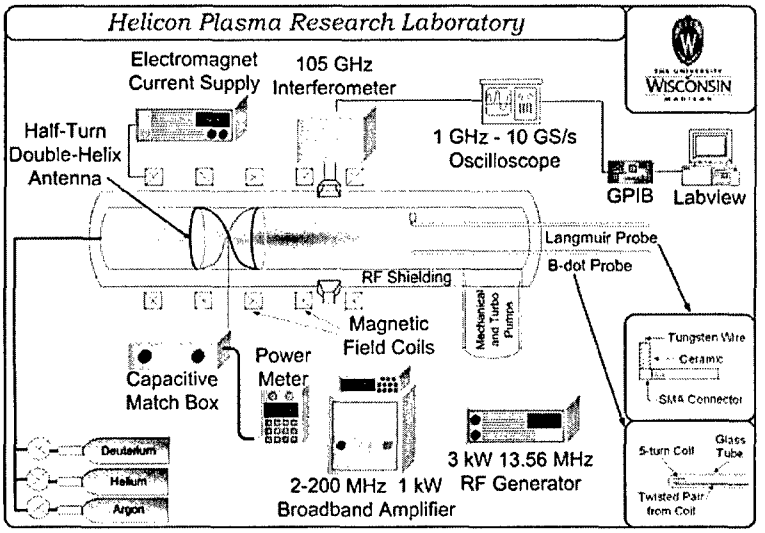

Figure 22. Magnetized Plasma Research Laboratory.

Experimental Results

The radial density profile is measured via a dogleg Langmuir probe in each of the three gases. The results of this measurement are presented in Fig. 21.

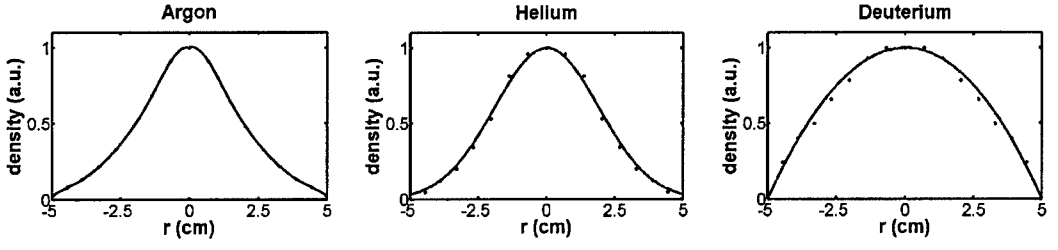

Figure 21. Radial density profiles in 3 mTorr argon, helium, and deuterium at 800 W input rf power and 600 G axial magnetic field.

Note that in argon the profile is more narrow, indicating good penetration of the rf power into the core of the plasma. Helium also exhibits significant radial peaking. Deuterium is significantly more radially diffuse, indicating that the deposition of power is different from the other two gases. These profiles may be explained by differences in the relative strengths of the radial modes.

The wave propagation is measured with the B-dot probe. The magnitude and phase measured along the axis at a radius of 2.5 cm is presented in Figure 22:

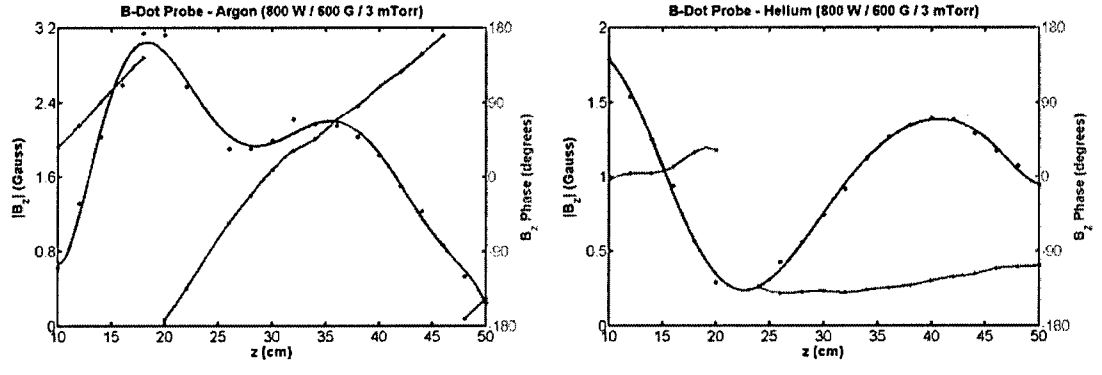

Figure 22. B-dot probe data of wave B_z for argon and helium discharges at 800 W, 600 G, and 3 mTorr

Both the argon and helium data exhibit minima and maxima in the rf amplitude along the axis as opposed to a monotonic decay away from the antenna (the edge of the antenna is at z = 0 cm). The wavelength in argon is significantly shorter than that in helium, evidenced by the sharper slope in the phase curve. The wave power seems to extend further axially in the helium plasma, indicating a stronger spatial absorption in argon (large k_i). Future research will include a more detailed measurement of radial wave modes, and an investigation into the role of ion and neutral mass on wave propagation and power deposition.

V. Future Research

We will concentrate on obtaining plasma at higher pressures in air and on obtaining plasma impedance variations during a laser-RF pulse so that moderate bandwidth, instantaneous matching can be obtained, as is described in our DURIP proposal that has recently been funded. We will also work on improving measurements of the plasma spectrum, optical measurements of plasma density, electron temperature, recombination rates and collisionality. We will initiate an experiment utilizing a laser focused and ionized air plasma located near a microwave window to examine the nano-physics of high-power breakdown in cooperation with MURI groups. Laser ionization of air has been shown to follow the same breakdown condition as microwave plasmas and is therefore relevant to the microwave window breakdown problem.

A technique for creating and diagnosing electrodeless, high-pressure, large-volume ($\geq$ 500 cm3) plasmas in argon (760 Torr) and nitrogen (50 Torr) is presented. The use of the readily ionized TMAE seed gas with UV excimer laser initiation allows the formation of plasma at high pressure with substantially reduced rf power levels. The laser frequency $f_{Laser}=1.55 \times 10^{15}$ Hz is much greater than the effective collision frequency $\nu=1.0 \times 10^{11}$ Hz for these high pressure plasmas. This allows excellent penetration of the laser into the high collisionality plasma and creates a long 100 cm plasma initial condition for the RF power coupling. Although the RF frequency $f_{RF}=1.356 \times 10^{7}$ Hz is much less than the $\nu \sim 10^{11}$ Hz collisional frequency, the high power $f_L=1.55 \times 10^{15}$ Hz laser-formed long plasma initial condition allows better penetration of the RF power and creation of a longer plasma that allows the plasma to

project well beyond the helical coil than would be possible with RF power alone. Broadband optical spectroscopy is utilized to illustrate the transition from the TMAE-seeded, laser-initiated plasma to the majority gas plasma later in the pulse sequence. A technique for accurate measurement of the helical antenna plasma impedance, which enables greatly improved rf matching via the two capacitor matching system with pulsed operation, is discussed and demonstrated. Power reflection levels as low as 5% are achieved. In addition, an interferometer technique to determine the electron temperature in neutral dominated high pressure plasmas is presented. The plasma impedance, electron density, effective electron neutral collision rate and electron temperature are systematically diagnosed and presented for both argon and nitrogen. The transition between the laser initiation and steady-state rf plasma is 130 ms for the 760 Torr argon case and 50 ms for the 50 Torr nitrogen case. The steady-state rf power density for the argon plasma is 5.0 W/cm^3 at 4.5×10^{12}/cm^3 at 760 Torr with an electron temperature of 1.3 eV. The steady-state rf power density for the nitrogen case at 50 Torr is 5.5 W/cm3 at line average densities of 1.4×10^{11}/cm^3 with an electron temperature of 1.0 eV.

We are examining additional techniques to improve the rf matching and transition time from the UV seed initiation to the steady-state rf plasma. These include the use of a wider footprint UV seed ionization pulse to fill the 5 cm diameter chamber, the use of vortex gas injection to stabilize the high pressure plasma discharges, and rf coupling at increased power levels.

Acknowledgements- This research was supported by AFOSR Grant No. F49620-03-1-0252. We thank Dr. Kamran Akhtar for many useful discussions and John Morin of Comdel, Inc. for useful technical assistance on the rf generator.

VI. Grant Modalities

During the grant period, the participants carrying out the research were as follows:

1. John E. Scharer, Professor, Co-Director, Center for Plasma Theory and Computation.
2. Kamran Akhtar, Postdoctoral Researcher, accepted in 10/05 a Plasma Scientist position with Blacklight Power of Princeton, NJ, a hydrogen plasma fuel cell company.
3. Mark Denning, Graduate Student, received a Richardson Distinguished Fellowship for 2004, has completed all courses and is currently a Ph. D. dissertator.
4. Siqi Luo, Graduate Student, has completed all courses and will become a Ph. D. dissertator in June 2006.
5. Magesh Thiyagarajan, received the IEEE Plasma Sciences Graduate Scholar Award for 2004, Graduate Student, has completed all courses and will become a Ph. D. dissertator in June 2006.

VII. References

[1] P. Tsai, L. Wadsoworth, and J.R. Roth, "Surface Modification of Fabrics Using a One-Atmosphere Glow Discharge Plasma to Improve Fabric Wettability," *Text. Res. J.* vol. 67, pp. 359, 1997.

[2] K. Kelly-Wintenberg, T.C. Montie, C. Brickman, J. R. Roth, A. K. Carr, K. Sorge, L. C. Wadsworth, and P.P. Y. Tsai, "Room Temperature Sterilization of Surfaces and Fabrics with a One Atmosphere Uniform Glow Discharge Plasma," *J. Ind. Microbiol. Biotechnol.*, vol. 20, pp. 69, 1998.

[3] K. Kelly, J.E. Scharer, G. Ding, M. Bettenhausen, and S. P. Kuo, "Microwave reflections from a vacuum ultraviolet laser produced plasma sheet," *J. Appl. Phys.*, vol. 85, pp. 63, 1999.

[4] R. J. Vidmar, "On the use of atmospheric pressure plasmas as electromagnetic reflector and absorbers," *IEEE Trans. Plasma Sci.*, vol. 18, pp. 733, 1990.

[5] M. Laroussi, "Scattering of EM Waves by a Layer of Air Plasma Surrounding a Conducting Cylinder," *Int. J. Infrared Millim. Waves*, vol. 17, pp. 2215, 1996.

[6] K. H. Becker, U. Kogelschatz, K. H. Schoenbach and R. J. Barker, *Non-Equilibrium Air Plasmas at Atmospheric Pressure*. Bristol: Inst. Phys, 2005.

[7] R.J. Vidmar and Kenneth R. Stalder, "Air chemistry and power to generate and sustain plasmas: Plasma lifetime calculations", in *Proc.* AIAA, 2003, pp. 1-8.

[8] M. A. Lieberman and A. J. Lichtenberg, *Principles of Plasma Discharges and Materials Processing*, 2nd ed. New York: Wiley, 2005.

[9] S. P. Bozeman and W. M. Hooke, "Magnetically enhanced electromagnetic wave penetration in weakly ionized plasmas," *Plasma Sources Sci. and Technol.* vol. 3, pp. 99, 1994.

[10] Andrei B. Petrin "On the Transmission of Microwaves through Plasma Layer," *IEEE Trans. Plasma Sci.*, vol. 28, pp. 1000, 2000

[11] H. U. Eckert and F. L. Kelly, "Spectroscopic Observations on Inductively Coupled Plasma Flames in Air and Argon," *J. Appl. Phys.*, vol. 39, pp. 1846, 1968.

[12] G. I. Babat, *J. Inst. Electron. Eng.* 94, 27 (1947).

[13] S. Ramakrishnan and M. W. Rogozinski, "Properties of electric arc plasma for metal cutting," *J. Appl. Phys. D*, vol. 60, pp. 2771, 1986.

[14] A. Schutze, J. Y. Young, S. E. Babayan, J. Park, G. S. Selwyn, and R. F. Hicks, "The atmospheric-pressure plasma jet: A review and comparison to other plasma sources," *IEEE Trans. Plasma Sci.*, vol. 26, pp. 1685, 1998.

[15] K. Akhtar, J. Scharer, S. Tysk and C. M. Denning, "Characterization of laser produced tetrakis (dimethylamino) ethylene plasma in a high-pressure background gas," *IEEE Trans. Plasma Sci.*, vol. 32, pp. 813, 2004.

[16] K.L. Kelly, J.E. Scharer, E.S. Paller and G. Ding, "Laser ionization and radio frequency sustainment of high-pressure seeded plasmas," *J. Appl. Phys.*, vol. 92, pp. 698, 2002.

[17] G. Ding, J. E. Scharer, and K. Kelly, "Diagnostics and analyses of decay process in laser produced tetrakis (dimethyl-amino) ethylene plasma" *Phys. Plasmas,* vol.8, pp. 334, 2001.

[18] K. L. Kelly, "Laser ionization and radiofrequency sustainment of high-pressure seeded plasmas," PhD thesis, Univ. of Wisconsin, Madison, WI, 2001.

[19] K. Akhtar, J. Scharer, S. Tysk, and E. Kho, "Plasma interferometry at high pressures," *Rev. Sci. Instrum.*, vol. 74, pp. 996, 2003.

[20] F. F. Chen, *Introduction to Plasma Physics and Controlled Fusion*, Rev. ed. New York: Plenum Press, 1984.

[21] A. Zecca, G. P. Karwasz and R. S. Brusa, "One century of experiments on electron-atom and molecule scattering: a critical review of integral cross sections," *Rivista Del Nuovo Cimento*, vol. 19, N.3, 1996.

[22] I. P. Shkarofsky, T. W. Johnston and M. P. Bachynski, *The Particle Kinetics of Plasmas.* Netherlands: Addison-Wesley Publishing, 1966.

[23] S. Tysk, C. M. Denning, J. E. Scharer and K. Akhtar, "Optical, wave measurements, and modeling of helicon plasmas for a wide range of magnetic fields," *Phys. Plasmas*, vol. 11, N. 3, 2004.

[24] K. H. Becker, U. Kogelschatz, K. H. Schoenbach and R. J. Barker, *Non-Equilibrium Air Plasmas at Atmospheric Pressure.* Bristol: Inst. Phys, pp. 504. 2005.

VIII. Our Recent Plasma and Microwave Research Publications

A. Book publications

1. "Modern Microwave and Millimeter Wave Power Electronics," R.J. Barker, J.H. Booske, N.C. Luhmann, and G.S. Nusinovich, Eds. (IEEE Press and Wiley, publication in April 2005). A. Singh and J. Scharer contributed 50 pages of material on harmonic and intermodulation suppression for linearity in broadband traveling wave tubes.

2. "Non-Equilibrium Atmospheric Air Plasmas". K. Becker, U. Kogelschatz, R. Barker, K. Schoenbach, Editors, Our research group contributed 70 pages on laser initiation and radiofrequency sustainment of air plasmas and plasma diagnostics in Chapters 7 and 8 that was published by the Institute of Physics (IOP) in 2005. In addition, Professor Scharer was Chapter Master for Chapter 7 on High Frequency Air Plasmas.

B. Reviewed Journal Publications in Plasmas (2004-5)

1. Siqi Luo, John Scharer, Magesh Thiyagarajan and Mark Denning, "Measurements of Laser-Initiated, Radiofrequency-Sustained, High-pressure Plasma Discharges", 42 pages, submitted to IEEE Trans. Plasma Sci., (2006).

2. Kamran Akhtar, John E. Scharer, Shane M. Tysk and C. Mark Denning, "Characterization of laser produced tetrakis (dimethylamino) ethylene plasma in high-pressure background gas", IEEE Trans. Plasma Sci., **32**, 813-822 (2004) http://legolas.ece.wisc.edu/papers/Akhtar_04.pdf

3. Shane M. Tysk, C. Mark Denning, John E. Scharer, and Kamran Akhtar, "Optical, wave measurements, and modeling of helicon plasmas for a wide range of magnetic fields", Physics of Plasmas, Vol. 11, No. 3, March 2004, pp 878-887.

C. Conference Papers and Presentations (5/03-5/06)

1. John Scharer, Siqi Luo, Magesh Thiyagarajan, Kamran Akhtar and C. Mark Denning, "Efficient Creation of Laser Initiated, RF Sustained Atmospheric Pressure Range Plasmas*", IEEE Conference Record - Abstracts, 2005 IEEE International Conference on Plasma Science, IEEE Catalogue Number 05CH37707, Oral talk 5A2, page 263,Monterey, CA (2005).

2. Magesh Thiyagarajan, Siqi Luo, John Scharer, Kamran Akhtar and C. Mark Denning, "Optical Emission Measurements of Laser Initiated, RF Sustained High Pressure Seeded Plsmas", IEEE Conference Record - Abstracts, 2005 IEEE International Conference on Plasma Science, IEEE Catalogue Number 05CH37707, Poster 2P6, page 199, Monterey, CA (2005).

3. Siqi Luo, Magesh Thiyagarajan, John Scharer, Kamran Akhtar and C. Mark Denning, "RF Matching Time Resolved Impedance, Power and Interferometer Measurements of Laser Initiated, RF Sustained Atmospheric Pressure Plasmas", IEEE Conference Record - Abstracts, 2005 IEEE International Conference on Plasma Science, IEEE Catalogue Number 05CH37707, Poster 2P5, page 198, Monterey, CA (2005).

4. C. Mark Denning, John Scharer, "Diagnostics and Computational Modeling of Argon, Helium, and Deuterium Helicon Plasmas in Nonuniform Magnetic Fields", IEEE Conference Record - Abstracts, 2005 IEEE International Conference on Plasma Science, IEEE Catalogue Number 05CH37707, Poster 1P2, page 115, Monterey, CA (2005).

5. Mark Denning, John Scharer, Kamran Akhtar, Alex Degeling and Rod Boswell, "Wave and Optical Measurements of Helicon Plasmas for a Wide Range of Magnetic Fields", American Physical Society, Division of Plasma Physics, paper BO3 9,page 29, The American Physical Society Vol. 48, Savannah (2004).

6. Kamran Akhtar, John Scharer, Mark Denning, and Siqi Luo "Novel Techniques for the production of High-Pressure Air Constituent Plasmas", 31st IEEE International Conference on Plasma Science, June 28 - July 1, 2004, Baltimore, Maryland, USA.

7. Mark Denning, Shane M. Tysk, John E. Scharer, Siqi Luo, and Kamran Akhtar, "Optical, Wave Measurements, and Modeling of Helicon Plasmas Over a Wide Range of Magnetic Fields", 31st IEEE International Conference on Plasma Science, June 28 - July 1, 2004, Baltimore, Maryland, USA.

8. J. Scharer, A. Degeling, M. Denning, S. Tysk, K. Akhtar, R. Boswell, and G. Borg, "Observations of Spatially Constant Peak ArII Emission Phase Threshold at Higher Helicon Densities", 31st IEEE International Conference on Plasma Science, June 28 - July 1, 2004, Baltimore, Maryland, USA.

9. Kamran Akhtar, John Scharer, Shane Tysk, and Mark Denning, "Radio-Frequency Sustainment of Laser Initiated, High-Pressure Air Constituent Plasmas", 56th Annual Gaseous Electronics Conference, October 21-24, 2003, San Francisco, California, USA

10. S.M. Tysk, C.M. Denning, J.E. Scharer and M.K. Akhtar, "Experimental Measurements and Modeling of a Helicon Plasma Source with Large Axial Density Gradients", 56th Annual Gaseous Electronics Conference, October 21-24, 2003, San Francisco, California, USA.

D. Abstracts – ICOPS 2006.

1. OPTICAL DIAGNOSTICS OF LASER INITIATED, RF SUSTAINED HIGH PRESSURE SEEDED PLASMAS, Magesh Thiyagarajan, Siqi Luo, John Scharer, Mark Denning, Electrical and Computer Engineering Department, University of Wisconsin-Madison 53706. POSTER 2P4Tuesday 6 June 1.00pm-3.00pm

2. DIAGNOSTICS AND SIMULATION OF HIGH-PRESSURE ARGON AND NITROGEN PLASMA, Siqi Luo, John Scharer, Magesh Thiyagarajan and C. Mark Denning, Department of Electrical and Computer Engineering, University of Wisconsin-Madison. ORAL 3D3 Tuesday 6 June 9.30AM

3. MEASUREMENTS ON AN ARGON HELICON PLASMA WITH VARIABLE MAGNETIC NOZZLE, C. Mark Denning and John E. Scharer, Dept. of Electrical and Computer Engineering, University of Wisconsin-Madison, Madison, WI 53706 USA. POSTER 1P72 Monday 5 June 1.00 - 3.00pm.